DYNAMIC ANALYSIS OF COMPOSITE OVERWRAP PRESSURE VESSEL

By

Shaojun Qiu

Thesis

Submitted to the faculty of the

Graduate School of Vanderbilt University

in partial fulfillment of the requirements

for the degree of

MASTER OF SCIENCE

in

Mechanical Engineering

December, 2004

Nashville, Tennessee

Approved:

Professor Kevin K. Tseng

Professor Sanjiv Gokhale

ACKNOWLEDGEMENTS

This research was completed with many thanks to my advisor, Dr. Kevin Tseng, for his guidance and encouragement throughout the course of my thesis. I would also like to thank Dr. Frampton for his encouragement.

TABLE OF CONTENTS

Page

.

LIST OF FIGURES

LIST OF TABLES

CHAPTER I

REVIEW ON HEALTH MONITORING OF COMPOSITE MATERIALS

Introduction to COPV

Composite Overwrap Pressure Vessel (COPV) has increasingly been used in many structural systems for automobile, aerospace, and aeronautical applications. The composite overwrap increases the pressure carrying capacity of the vessel without adding too much weight to the tank.

The composite overwrap is typically in the form of laminates with multiple layers of unidirectional carbon fibers. This class of composite material is relatively new to the engineering communities and their material behaviors are not as well understood as traditional materials such as metals and metallic alloys. To ensure safe operation of the structural system consisting COPV, an on-line automatic structural health monitoring system is needed to constantly monitor the integrity of the structure.

Many structural health monitoring techniques have been proposed. Most of these techniques are based upon global or local dynamic characteristics of the structure or material. The structural health monitoring system identifies changes in the global or local dynamic characteristics and issues warnings or triggers structural control system to bring the structural performance back to normal. This kind of hybrid sensing/control system can be achieved by using proper smart materials such as the piezoceramics.

The purpose of this project is to test the feasibility of predicting working conditions of a structure based on the change of their dynamic characteristics. The analyses are divided to two categories: an aluminum tank, and the aluminum tank overwrapped with carbon fiber composite materials. For both categories, the tank is filled with water, both with and without pressure.

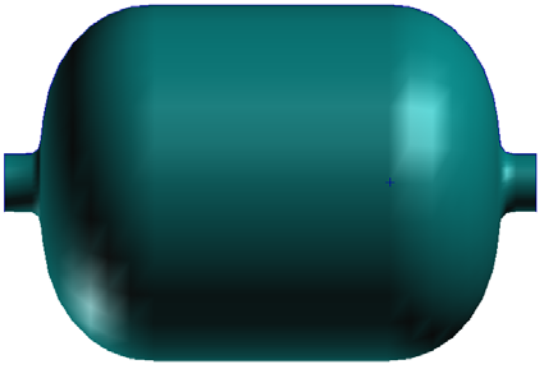

Figure 1. Pressure vessel used in this study

The composite overwrap pressure vessel (COPV) used in this project is made of aluminum alloy and the overwrap is laminated unidirectional carbon fibers. The tank is 22.25 in. in length and center part has an inner radius of 14.92 in (Figure 1). The cylindrical part of the vessel is wrapped with 5 hoop layers of carbon fibers and 2 helical layers cover the entire tank.

Composite overwrap greatly increases pressure carrying capacity of the vessel without adding too much weight to the tank. Experiments at NASA Marshall Space Flight Center show that the burst pressure of an aluminum tank can be increased from 500 psi to 2,850 psi when the tank is wrapped with 5 layers of carbon fiber composites.

Dynamic and Strength Analysis of Composite Pressure Vessel

When a pressure vessel is overwrapped with composite materials, both its dynamic and strength characteristics change dramatically. Sun et al. [3] used finite element methods to investigate the fundamental frequencies of laminated anisotropic circular cylindrical composite shells, based on extended Sanders' first order shear deformable shell theory.

Su [4] used a three-dimensional finite element (FE) method to study the effect of composite wrapping on the fracture behavior of the steel-lined hoop-wrapped cylinders. The influence of the hoop-wrapped materials, the internal pressure and the crack sizes on the fracture behavior of the cylinder are discussed. It was found that the transverse modulus of elasticity of composites plays a key role in the strengthening of the gas cylinders. Kisioglu [5] used both experiment and FEA approaches to determine the burst pressure of DOT-39 refrigerant cylinders. The prediction of the BP (burst pressure) in filament-wound composite vessels was studied using neural network acoustic emission testing by Hill *et al*. [6], and using the finite element method proposed by Sun *et al*. [7]. The plastic deformation and burst of the multilayered cylinders was developed analytically using elastoplastic finite strain theory under generalized plane strain by Tadmor and Durban [8] and Blandford *et al*. [9]. The BP of a vessel was estimated after a single application of internal pressure using mathematical and experimental models for tensile loading by Updike and Kalnins [10]. Xia [11] presents a simplified elastic solution to analyze the stress and deformation of multi-layered filament wound composite pipes under internal pressure. Detailed stress and displacement distributions for designs with different angle-ply pipes under internal pressure load are investigated. Conder [12] described a test program whereby a filament wound vessel filled with liquid nitrogen was

subjected to 2000 pressure cycles to 3000 psi without degradation of the structural capability of the vessel. It was concluded that the cryogenic cycling and the vacuum environment (the vessel was put in a vacuum jacket) did not degrade the structural strength of the vessel. The vessel was constructed using an aluminum liner overwrapped with Kevlar-epoxy reinforcement.

Hwang [13] conducted probabilistic analysis and experimental tests to predict the probabilistic deformation and strength (strain and burst pressure) of carbon/epoxy composite pressure vessels subjected to internal pressure loading. A computer code was utilized for the progressive failure analysis. Kamat [14] used GENOA Progressive Failure Analysis (GENOA-PFA) for simulations of the manufacturing process and subsequent assessment of COPV durability and damage tolerance. GENOA-PFA is virtual design/analysis software capable of simulating progressive failure of composite structures in a variety of situations. Optimization of winding process and ply lay-up for COPV design were also investigated.

Fluid-structure Interaction

The study of the interaction between liquid and structure during vibration is of great interest. A wide literature is available, regarding the case of shells with a vertical axis completely or partially filled with liquid. But for a simply supported cylindrical shell with the axis placed horizontally and partially filled with liquid, the work is limited. This is a typical configuration in engineering and constitutes a rather complex problem because of

the lack of axial symmetry. Amabili and Dalpiaz [15] experimentally studied this problem.

Pal [16] used finite element method to simulate the effects arising from the non-linear motion of the liquid free surface, due to sloshing, in a partially filled laminated composite container, along with the associated coupling due to fluid–structure interaction. Amabili [17] performed experimental modal analysis on an empty and water-filled, circular cylindrical tank horizontally suspended. The effect of the fluid in a simply supported tank is a large reduction of the natural frequencies of the shell because of the added mass of the fluid.

In some applications, the vibration response of cylindrical shells calculated by linear theory is inaccurate. When the vibration amplitude becomes comparable to the shell thickness, a nonlinear theory should be used. The effect of the fluid is to enhance the nonlinear character of shell vibration. A strongly softening behavior is found for a fluid-filled shell. Hence, nonlinear analysis could be more important for fluid-filled shells than for empty ones. Amabili [18] investigated the nonlinear free and forced vibrations of a simply supported, completely filled circular cylindrical shell in contact with an incompressible and inviscid, quiescent and dense fluid. Donnell's shallow-shell theory is used, so that moderately large vibrations are analyzed. Amabili [19] investigated the large-amplitude response of simply supported cylindrical shells to a harmonic excitation in the spectral neighborhood of one of the lowest natural frequencies. The effect of internal quiescent, incompressible and inviscid fluid is investigated.

Amabili [20] presented an analytical solution to the free vibration problem of cylindrical shells half-filled with liquid, and with the shell axis orthogonal to the gravitational field. Approximate models were proposed to estimate natural frequencies and mode shapes of partially filled shells. The presence of a liquid in a shell structure has a great effect on its modal characteristics. In the case of partial filling, with the presence of a free liquid surface parallel to the shell axis, the circumferential mode shapes are modified.

Dynamics of Composite Materials

Composites are complex materials exhibiting distinct anisotropic properties. Singh [21] and Saravanos [22] investigated the damping of composite cylindrical shells and plates. Maeda [23] presented an experimental investigation on the vibrational characteristics of angle-ply laminate made of carbon/epoxy composite material. Kadoli et al [24] studied the effect of axisymmetric temperature variation on the variation of free vibration natural frequencies and active damping ratios, based on FEA. The models are isotropic and orthotropic cylindrical shells with bonded piezoelectric material on the inner and outer surface of the shell lamina. Parhi [25] investigated the hygrothermal effects on the dynamic behavior of delaminated composite plates and shells. Rise in moisture and temperature reduces the elastic moduli of the material, reduces the fundamental frequency and induces internal initial stresses. To compensate frequency reduction due to hygrothermal effects, Rajaa [26] used PZT actuators for active stiffening of angle ply laminates based on FE modeling. Detwiler [27] developed a finite element formulation to analyze the mechanical-electrical behavior of laminated composite structures containing distributed piezoelectric actuators and sensors.

Effect of Delamination on Dynamic Modal Parameters

Common damages for composite materials are matrix cracking, fiber breakage, fibre-matrix debonding, and delamination between plies [1]. Delamination, probably the most frequently occurring damage, appears as a debonding of adjoining plies in laminated composites. The causes of delamination such as imperfect bonding, crack in matrix materials, separation of adjoining plies, and broken fibers may originate during manufacturing. Alternatively, delamination may be induced during in-service loading, such as by foreign object impact or by fatigue.

Delamination changes structural dynamic characteristics. Saravanos [28] investigated the effects of delaminations on the dynamic characteristics of composite laminates, including damping, analytically and experimentally. Tracy and Pardoen [29], Nagesh Babu and Hanagud [30], Paolozzi and Peroni [31], and Shen and Grady [32] have analyzed the effects of a single delamination on the natural frequencies and modes of composite beams using the "four-region" approach; that is, the delaminated beam was divided into four regions and beam theory was applied to each region. Tenek *et al*. [33] used a similar approach for plates. On a parallel approach, Anastasiadis and Simitses [34] and Simitses [35] have addressed the buckling of delaminated beams. Barbero and Reddy [36] developed a finite element model using layer-wise theory for the analysis of delaminated laminates. This modeling is further improved by a higher order theory with enhanced strains to describe layer-wise displacements more accurately [37]. The layer-wise plate theory was later extended by Lee et al. [38] on a finite element based buckling analysis of composite beams with multiple delaminations. A laminated shear deformable beam finite

element model was developed for analyzing the growth of dynamic delamination [39]. The delaminated beam was modeled as two beams above and below the plane of delamination. Beam finite elements with nodes offset to the bottom and top are used to model the top and bottom sublaminates respectively. This concept is further developed by dividing the delaminated part of the beam as three beam finite elements, which are connected at the tip of delamination by additional boundary conditions [40]. The advantage of this method is that it can be easily modified to accommodate different types of damage.

In general, delaminations decrease the stiffness and increase the damping of the structure. These, in turn, decrease the frequencies and increase modal damping in delaminated structure. The existence of the "delamination modes" in composite beams has been proven theoretically and experimentally [41, 42] and it can be an important feature for delamination detection. For structural mass, the effects of delamination are usually very small and often can be neglected.

Frequency

The effect of delamination on the natural frequencies of composite beam laminate structure depends on the size and location of the delamination. It has been found [29] that all first four modes are unaffected for very short delaminations. Among the first four modes, mode 1 (lowest frequency) is insensitive to the presence of normal-sized delamination while mode 4 is most sensitive. The effect of delamination is much stronger in high shear regions than in high curvature regions. The study concludes that the extent

of frequency degradation in a particular mode of vibration caused by a delamination depends on the size and location of the delamination in the structure. It is also found that local delaminations do not have a noticeable effect on the global mode shape of vibrations of composite beams [43]. It is pointed out that the delamination caused frequency shift and the maximum frequency shifts occurred in the modes where the wavelength was approximately of the same size as that of the debonding area.

Damping

Damping is generally far more sensitive to delamination than stiffness is. This suggests that damping would be a better indicator of delamination damage especially in small and medium crack lengths. At small delamination sizes, changes in damping were caused primarily by changes in the viscoelastic laminate damping of the structure, while interfacial friction damping becomes important at large delamination cracks. Although it can be a better indicator, damping is a complex factor to consider.

Mode Shape

Delamination causes irregularity of mode shape curves. The extent of the irregularity of the curve depends on the size and location of the delamination [43, 44]. The bigger the delamination, the more irregular the mode shape curve. The closer to the surface of the structure the delamination, the more irregular the mode shape curve. Overall, small delamination (less than 10% of beam span) may not be detectable by monitoring global modal characteristics of the beam. Therefore, other local parameters should be monitored [28]. Finally, the effect of delamination on the dynamic characteristics of structures is

strongly dependent on the laminate configuration, and can be more profound in laminates with complex laminations [28].

Model-dependent Damage (Delamination) Identification

Currently available non-destructive evaluation (NDE) methods are mostly non-model methods, i.e., either visual or localized experimental methods, such as acoustic or ultrasonic methods, magnetic field methods, radiographs, eddy-current methods and thermal field methods. Accessing these techniques is time consuming and costly. Some of them are also impractical in many cases such as in service aircraft testing, and space structure. Almost all of these techniques require that the vicinity of the damage is known in advance and that the portion of the structure being inspected is readily accessible for human beings. Subjected to these limitations, these non-model methods can provide only local damage information and not global information.

Shortcomings of currently available NDE methods indicate a requirement of damage inspection techniques that can give global information on the structure and they do not require direct human accessibility of the structure. This requirement has led to the development of model-based methods that examine changes in the vibration characteristics or impedance of the structure and also led to the development of smart structures. Smart structures have the ability to detect damage on-line, and the capacity to locate the position of the damage, and to estimate its severity using sensor information.

The model-based methods undertake analysis of structural models and are usually implemented by finite element analysis. Damage is simulated by modifying the models. There are basically two approaches: vibration-based approach and impedance-based approach.

Vibration-based Approach

The vibration-based approach utilizes the PZT actuator to generate certain wave to propagate in the structure and compares the structural modal parameters (modal shape, modal frequency, damping, stiffness, etc.) or response curves (frequency response, time response, transfer function, etc.) with those of the healthy state to detect damage.

Modal Analysis Methods

This group of methods utilizes the information from all modal parameters (modal frequencies, mode shapes and modal damping ratio) or combinations of some of them to detect damage. The basic idea of these methods is that modal parameters are functions of the physical properties of the structure (mass, damping and stiffness). Therefore, changes in the physical properties, e.g., damage, will cause changes in the modal properties. Usually, damage will decrease the mass and stiffness of the structure and increase the damping ratio locally. According to their different detection techniques, the modal analysis methods can be divided into the following major categories: modal shape changes methods [45, 46], modal shape curve methods [48, 49], sensitivity-based update methods [49, 50], eigenstructure assignment methods [51, 52], optimal matrix update

methods [53, 54], changes in measured stiffness matrix methods [55, 56], frequency response function method [57, 58] [60,61], and combined modal parameters method [59].

The majority of this group of methods uses lower frequencies of the modal data that can best describe the global behavior of the structure. Because of their global nature, these techniques allow the customization of measurement points. Another major advantage is that the modal information is cheap to obtain and easy to extract.

However, there are some shortcomings in utilizing the structural modal parameters in health monitoring. These are: 1) modal-based method can only detect the particular forms of damage in their diagnostic schemes 2) modal-based method fails to detect small defects in global features.

Frequency Domain

Damage may be detected only using frequency response of the structure. The foundation of this group of methods is that damage produces a decrease in structural stiffness, which, in turn, produces decreases in natural frequencies. The damage location affects each mode differently. From the degree of change in natural frequencies, the location of the defect can be estimated. It was suggested [62] that monitoring local high-frequency modes of local area provide a better indication of damage for small damage. It was suggested that resonant frequency is a better indicator of defects than frequencies because it can change more significantly than frequencies do when properties change [62].

There are several other methods available in this frequency domain category such as the damage index method [63], the sensitivity analysis method, etc. [64, 65].

However, natural frequency changes alone may not be sufficient for the unique identification of the location of structural damage. The current frequency domain methods are either using lower frequencies for providing global information of structures or using higher frequencies for providing local information of structures. None of these can provide sufficient information for the detection of both small and large defects.

Time Domain

Basically, all methods in this category are related because they use time history. These methods could be independent of modal information although they are usually combined with frequency domain methods. Damage is estimated using time histories of the input and vibration responses of the structure. Using time response over a long period while at the same time taking into account the information in several modes so that the damage evaluation is not dependent on any particular one, could be sensitive to any modes [66]. The big advantage of the methods in this group is that they can detect damage situations both globally and locally by changing the input frequencies.

Impedance Domain-based Approach

Damage is detected through measuring the changes of impedance in the structure. The basis of this technique is that each part of the structure contributes to the impedance of structure to some extent. Any variation in the structure integrity will generally result in changes in the impedance. This group of methods is capable of multi-location and real-

time health monitoring [67, 68]. Impedance domain methods are particularly suitable for detecting planar defects such as delamination.

The impedance-based qualitative health monitoring technique is a real-time structural damage detection method. The initial work of the impedance-based health monitoring was proposed by Sun *et al* [69] on an assembled truss structure. Chaudhry *et al* [70] applied this method in local area health monitoring of aircraft by using piezoelectric actuators and sensors. Ayres *et al* (1998) [71] verified the usefulness of this method for a 226,80 kg structure quarter-scale deck truss bridge joint. The mechanical impedance is measured indirectly through the electrical impedance of the PZT by using the electromechanical property of PZT. By converting the impedance measurements into a scalar damage index, the real-time implementation of the impedance-based technique has proven to be successful. In order to find optimal placement of the piezoelectric sensors for the impedance domain-based health monitoring, Esteban *et al*. (1999) [72] modeled the wave propagation generated by the PZT throughout the structure. The authors found out that due to high frequency of excitation, the sensing region of the PZT actuator-sensor was highly localized in the presence of energy dissipation mechanisms. However, this method is qualitative, not quantitative. Therefore, if the exact nature of damage is desired, other quantitative health monitoring method should be applied.

Tseng *et al*. (2002) [73] presented the results of an experimental study for the detection and characterization of damages using PZT transducers on aluminum specimens. The impedance characteristics of the PZT transducer are extracted to detect damage. Different

types of damages were simulated by drilling holes of various dimensions on aluminum specimens. The admittance (inverse of impedance) response of the PZT transducers was studied for change in damage location, damage extent, and damage size. Root-mean-square deviation (RMSD) between the signatures of two states is applied as damage index and was given by

$$RMSD(\%) = \sqrt{\frac{\sum_{i=1}^{i=N}(y_i - x_i)^2}{\sum_{i=1}^{i=N} x_i^2}} \times 100$$

where x_i and y_i ($i=1, 2, 3,\ldots,N$) are signatures obtained from the PZT bonded to the structure before and after the damage. The experimental results showed that the higher frequency ranges were more sensitive in characterization. The RMSD values of different specimens showed that the PZT transducer has a very high sensitive to detect damages located at the specimens. The advantage of the impedance detection method over the other modal analysis techniques is that it does not require the knowledge of the modal parameters of the structure.

On-line Delamination Detection

To implement the on-line monitoring techniques, an essential condition is making the structure smart or the material intelligent.

Smart Structure

A smart structure/intelligent material system contains a network of sensors and actuators, real-time control capabilities, computational capabilities and a host structural material. The system can inspect the health conditions of the structure automatically and

continuously by itself. The actuator induces actuation into the structure, such as vibration through strain or displacement. The sensors recognize and measure the signal, such as the resultant vibrational response. Information from the sensors is acquired by the control/processor unit.

Application of Piezoelectric Materials

There are a number of sensors and actuators available for use in smart materials, and systems. Among them, piezoelectric materials offer a number of advantages. Piezoelectric materials can generate a charge in response to mechanical stimulus, or alternatively provide a mechanical strain when an electric field is applied across them. Due to their low mechanical impedance, a number of piezoelectric films/patches can be distributed along the structure with only minor effects on the structure's mechanical properties. The films/patches can be readily cut and shaped to conform to the structure under consideration. They are especially good for incorporating into composites, usually attached to or embedded into a structure. It is important to note that there is an optimum size and an optimum placement or arrangement of piezoelectric sensors to give maximum sensitivity for the various damage cases and load conditions [74-78]. Research on piezoelectric single crystals, such as PZN-PT and PMN-PT, in which very high strains can be induced, were investigated for electromechanical actuators [79].

On-line Health Monitoring with Piezoelectric Transducer

The group of on-line delamination detection techniques is used to monitor changes in the dynamic characteristics or in the dynamic response of a structure. The group of techniques usually uses algorithm for finite element model update or test-analysis

correlation. Most of these works begin with measured dynamic response and modal parameters to find the differences between the undamaged and damaged system. There have been a few attempts at on-line delamination detection using piezoelectric sensors and actuators. Most of them are combined with Artificial Intelligence-based techniques such as neural network.

Wang *et al* (2001) [80] developed a built-in network of piezoelectric materials for health monitoring of fiber-reinforced composites and steel-reinforced concrete. The authors presented an active sensing diagnostic system that contained a network of piezoceramics used as both actuators and sensors to generate and acquire ultrasonic stress waves in the plates. The authors did the health monitoring on composite plates and steel reinforced concrete. To detect delamination in the composite plates, a five-peak, narrow-band, modulated sinusoidal burst waveform over a wide range of frequencies was selected for the actuator. The experiment results showed that delamination in composites could significantly reduce the sensor signal strength and arrival time as compared with the healthy state sensor signals. When a propagating wave encounters an area where there is a change in material properties, scattering occurs in all directions. The X-ray examination was implemented on the fiber-reinforced plate and the X-ray images were consistent with the result.

An on-line damage diagnostic technique was applied for predicting delamination with piezoelectric sensors and actuators attached to the top and bottom of a beam and validated by experimental works [81-83]. This diagnostic scheme is a search-based

technique with an iterative damage identification algorithm combined with a wave response and a frequency domain method. This damage identification technique includes three components, a structural model, a response comparator and a damage selector. The structural model was also applied to detect impact delamination [84] and further for self-monitoring of the manufacturing process and self-diagnosis of service-induced damage [85].

An electromechanical structural model combined with neural network was used to conduct on-line delamination detection on composite structures with embedded piezoelectric sensors and actuators [86]. The structural model was an extension of the Tracy and Pardoen modeling of delamination [29] by including unsymmetrical laminates and effects of embedded piezoceramic patches. This model was validated by both experimental and numerical works. A good match was found in the case of mode shape verification. Detecting the presence of damage still called for a conventional technique. Two methods are used to locate the damage position and determine the type and size of damages. The first method compared numerical with experimental frequency results. The second method used a back-propagation neural network, which is trained by the frequencies of the first five modes obtained from dynamic modal analysis data. It was pointed out that the embedded actuator patches, in addition to acting as exciters, have the potential to redistribute strain for damage mitigation.

Another Artificial Intelligent- (AI) based damage detection technique was proposed [87]. This technique combined modal analysis with neural network. The delamination is

modeled by the structural model of the Mujumdar and Suryanarayan [88] without considering the effect of PZT patches. The presence and location of delamination were identified by comparing theoretical and experimental results. The size of delamination was estimated by neural network. It was found that the third and fourth modal frequencies were better indicators of delamination detection. The efficiency of this method was demonstrated experimentally.

A neural network method in conjunction with system identification technique [89], which can identify various damage cases, was applied for on-line damage detection in composite structures. The method contains two parts: training and recognition. In the training part, various types of damage modes are designed as the patterns and organized into pattern classes according to the location and the severity of the damage. Then system identifications are used to extract the transfer functions as the features of the structural systems. The multi-layer perception (MLP) was trained by the transfer functions. The MLP serves as a nearest-neighborhood classifier. In the pattern recognition part, an unforeseen damage in a structure is classified within the closet class in the training set and the damage in the structure is identified as that of the class.

There are many other valuable studies using neural networks to detect delamination in composite structures, such as an experimental study [90] for a composite/aluminum beam to identify the severity and presence of a delamination according to the frequency response data obtained from bonded piezoelectric actuators/sensors. This experimental work also investigated the effectiveness of different configuration of network. Another

example is the dynamic learning rate steepest descent method [91]. This method can improve learning convergence speed significantly without increasing the computational effort, the memory cost, the algorithm simplicity, and the computational locality in the standard layered error back-propagating training algorithm.

Signal Processing Method for the Health Monitoring Utilizing PZT

To effectively extract the damage information, the sensor signal is processed by different methods to analyze the data. In recent years, wavelet analysis and artificial neural network have been successfully applied to detect delamination of composites and for health monitoring of reinforced concrete.

Application of Wavelet Analysis to PZT-based Health Monitoring

Wavelet analysis has recently emerged as a promising tool for structural health monitoring (SHM) and damage detection. The wavelet transform can decompose the structural vibration response signals into multiple sub-signals. The change corresponding to structural damage in each sub-signal may manifest notable differences, and some of the sub-signals may possess high sensitivity to minor damages in structure.

Hou et al (2000) [92] presented a wavelet-based approach for SHM and damage detection. The research results showed that the structural damage or a change in system stiffness may be detected by spikes in the details of the wavelet decomposition of the response data. The locations of these spikes may accurately indicate the moments when the structural damage occurred.

Lin et al (2001) [93] modeled the diagnostic transient waves in an integrated piezoelectric sensor/actuator plate with a view to use it as a first step towards establishing an entire structural health monitoring system and to provide experimental verification of the proposed models. PZT ceramic disks were surface mounted on an aluminum plate to generate and collect Lamb waves. Mindlin plate theory was adopted to model the propagating waves by taking both transverse shear and rotary inertia effects into account. The authors also presented experimental results to show that single-mode Lamb waves in the plate can be successfully generated and collected through the integrated PZT disks. Na et al (2003) [94] showed that the Lamb wave can propagate a long distance and is sensitive to damage inside. Therefore, PZT-based method incorporated with the Lamb waves is a promising approach for health monitoring of large-scale structure.

In order to detect the delamination in the composites, Lemistre M et al. (2001) [95] proposed a multiresolution process by discrete wavelet transform (DWT) with an orthonormal basis. A health monitoring system was presented composed of integrated disc-shaped, 100 μm thick and 5 mm diameter piezoelectric transducers (PZTs) working sequentially as Lamb wave emitters and receivers. The peculiarity of the DWT is that each result obtained with each daughter wavelet corresponds to the time behavior of the signal in a frequency band. Location and identification of damage like delamination, fiber fracture and matrix cracking in various composite materials are difficult due to the presence of high-amplitude interfering echoes mixed within the main signal. The authors proposed the time delay equation to locate the delamination. The proposed method (for

each resolution) gives a possible damage localization point. The results matched with the exact location of damage determined by ultrasonic examination.

Application of Artificial Neural Network (ANN) to PZT-based Health Monitoring

There have been a lot of successful applications of artificial neural network in the health monitoring. This is because artificial neural network has a particular advantage in establishing mapping relationships between feature proxy and physical parameters of structural damage. When classifications and identification of structural damage is carried out, the required task is only to train the ANN in advance using a set of known damage feature proxy and damage physical parameters of the structures to be detected.

Yam et al (2003) [96] presented an integrated method for damage detection of composite structures using their vibration responses. Vibration signals were decomposed by wavelet packet algorithm and the mapping relationships between the structural damage feature proxy and damage status (location and severity) was established by artificial neural networks.

Delamination is of particular interest in health monitoring because it can cause catastrophic failure of the composite structure. Okafor et al (1996) [97] conducted modal testing of a perfect beam and beams with different delamination by using polyvinylidene fluoride film (PVDF) as sensor and PZT patches as actuators. Back propagation neural networks were trained on the basis of the modal frequencies of the beam. The

experimental results showed that neural network models developed successfully predict the delamination size in the composites.

Although the neural network has the advantage of not requiring a prior knowledge of the system, it also has the shortcomings such as lack of precision and the limited ability to rationalize solutions. The neural network may not respond properly to the data which is not related to the training data. Therefore, if the training data does not contain enough information, the neural network may not work properly in practice.

Other Applications of Piezoelectric Materials in Structural Health Monitoring

Piezoelectric paint film sensor has the advantage that the paint is readily applied over large areas of a structural material without drastically affecting its mechanical properties. The paint can be applied even to complex shapes of a structural material. Egusa et al (1998) [98] prepared piezoelectric paints using PZT ceramic powder as a pigment and epoxy resin as a binder. The experimental results proved that the piezoelectric sensitivity of the paint film is high enough to determine the natural frequencies and mode shapes of the underlying structural material, thus demonstrating the potential of the paint film as a vibration modal sensor. Galea et al (1993) [99] also successfully applied the piezoelectric films in detecting and monitoring damage in composites.

Conclusions

Impedance domain-based approach and vibration-based approach are two major categories of PZT-based health monitoring. The principle of impedance-based method is that the measured electrical impedance of the PZT patch is directly related to the mechanical impedance, and will be affected by the presence of damage. The impedance domain methods are particularly suitable for detecting planar defects such as delamination.

The principle of vibration-based approach is to detect the damage by comparing the model parameters or response curve with the healthy structure under the excitation of a certain vibration source. This method consists of modal analysis method and frequency domain method. The modal analysis methods are based on the concept that modal parameters are functions of physical properties, which will change if the damage exists. The most important task in detecting damage with these methods is to find the particular modes which best describes the individual damage event.

Frequency domain methods use only frequency information for damage detection. However, natural frequency changes alone may not be sufficient for a unique identification of the coordinates of structural damage.

It is very important to apply a proper signal-processing tool to analyze the sensor signal for the health monitoring purpose. Artificial neural network and the wavelet analysis are the useful tools to analyze the vibration signal of PZT sensor to detect and analyze the

delamination, crack or other damages in large-scale structures. In health monitoring of structures, neural networks and wavelet analysis are usually combined with modal analysis or frequency domain analysis to extract the feature of damage information. Successful applications of neural network and wavelet analysis in the PZT-based health monitoring have been reviewed. The advantage of neural network is that this method does not require too much prior knowledge. The advantage of wavelet analysis is that it can detect small cracks or other very low extent damages by analyzing the vibration signals. This is because wavelet analysis enables the inspection of relatively narrow frequency bands over a relatively short time window. Neural network and wavelet analysis incorporated with the piezoelectric sensors and actuators provides a promising option for the health monitoring of large-scale structure.

Although piezoelectric materials are promising and have great potential in the health monitoring of large structures, there exists some challenges in this field. The main focus of health monitoring is to locate precisely the damage and assess the severity of the damage. Because the defect may diffract the wave propagation in every direction, the exact location is difficult to assess. Different types of damage may have similar effect on the response of piezoelectric materials; therefore the extraction of the type of damage remains a challenging task.

CHAPTER II

DYNAMIC MODELING OF PRESSURE VESSEL

Since the dynamic characteristics of a structure may be used to identify the working conditions of the structure, we want to see how the dynamic characteristics change in different conditions. For Chapter II and III, we will discuss how the dynamic properties of a pressure vessel change when it is empty, filled with water, and overwrapped with composite materials, respectively.

The pressure vessel (PV) used in this research is made of aluminum alloy and the overwrap is laminated unidirectional carbon fibers. The tank is 22.25 in. in length and the center part has an inner radius of 14.92 in. The cylindrical part of the vessel is wrapped with 5 hoop layers of carbon fibers and 2 helical layers cover the entire tank. In this study, both the underlying theory and finite element analysis were performed.

Mathematical Model

In vacuo Analysis

Firstly, the empty (*in vacuo*) tank is discussed. The equation of motion describing the response of a flexible structure to external excitation may be written as [100]

$$M\ddot{U} + C_v\dot{U} + KU = F \tag{1}$$

Where M, C_V, K denote the mass, structural damping and stiffness matrices, respectively. The vectors **U**, $\dot{U}$ and $\ddot{U}$ represent the structural displacements, velocities, and accelerations, respectively, and the column vector F denotes the external forces.

In an *in vacuo* analysis, the structure is assumed to vibrate in the absence of any structural damping and external forces. Equation (1) is reduced to the form

$$M\ddot{U} + KU = 0 \tag{2}$$

The form of equation (2) suggests that one can express the trial solution as

$$U=De^{i\omega t} \tag{3}$$

Substituting equation (3) into equation (2) and canceling the common factor $e^{i\omega t}$, one obtains the following equation

$$(-\omega^2 M + K)D = 0 \tag{4}$$

Equation (4) describes the simple harmonic oscillations of the free undamped structure and the *in vacuo* principal modes and natural frequencies are determined from the associated eigenvalue problem.

Generalized Equation of Motion

The distortions of the structure may be expressed as the sum of the distortions in the principal modes,

$$U = D\ p(t) \tag{5}$$

where D is the modal matrix whose columns are the *in vacuo*, undamped mode vectors of

the structure. Matrix p is the principal response coefficients matrix. By substituting equation (5) into equation (1) and pre-multiplying by D^T, the following generalized equation in terms of the principal response coefficients of the structure is obtained:

$$a\ddot{p}(t) + b\dot{p}(t) + cp(t) = Q(t) \tag{6}$$

where **a**, **b**, **c** denote the generalized mass, damping and stiffness matrices, respectively, and are defined as

$$\mathbf{a}=\mathbf{D}^T\mathbf{M}\mathbf{D}, \quad \mathbf{b}=\mathbf{D}^T\mathbf{C}_V\mathbf{D}, \quad \mathbf{c}=\mathbf{D}^T\mathbf{K}\mathbf{D}, \quad \mathbf{Q}=\mathbf{D}^T\mathbf{P} \tag{7}$$

The generalized force matrix $\mathbf{Q}(t)$ represents the fluid–structure interaction force, and all other external forces.

Dynamic Analysis of Fluid-structure Interaction

Introduction

When a structure is in contact with a fluid of comparable density, such as water, the fluid loading which depends on the structural surface motions will significantly alter the dynamic state of the structure from that of the *in vacuo* vibration. The fluid–structure interaction can be considered as *feedback coupling*.

The dynamic fluid–structure interaction problems in which the fluid domain is modeled with finite elements are generally formulated using methods based on fluid particle displacement, or pressure, or velocity potential, etc., as the major unknown. These procedures are quite effective for problems involving a bounded fluid domain. For instance, Lim and Petyt [101] investigated the free vibration characteristics of a thin, circular cylindrical shell partially or completely-filled with water, using displacement potential and displacement as the fundamental unknowns, respectively, in the fluid and

structural domains. Alternatively, Olson and Bathe [102] used velocity potential as the major unknown in the fluid and presented a finite element method for solving fluid–structure interaction problems. Using appropriate variational formulations by means of the finite element method, Ohayon and Valid [103] and Morand and Ohayon [104] derived various symmetric matrix equations for the linear vibrations of elastic structures coupled to internal fluids. Mazúch et al. [105] used Ahmad shell elements with reduced integration for thin shells and quadratic fluid elements for an inviscid incompressible fluid, and calculated and measured the free vibration characteristics (i.e., natural frequencies, mode shapes, etc.) of a clamped–free cylindrical shell partially filled with water. More recently, Zhang et al. [106] presented a finite element method, based on Sanders' non-linear thin shell theory and the classical potential flow theory, for the vibration of initially tensioned thin-walled orthotropic cylindrical tubes conveying fluid.

Boundary integral equation methods are also widely applied for the fluid flow, together with a finite element method for the structure displacements. For example, Ergin [100] presented a boundary integral equation method in conjunction with the method of images, to investigate the dynamic behavior (wet frequencies and associated mode shapes) of fluid containing structures. Röhr and Möller [107] described a hydroelastic vibration analysis method based on a combined finite element–boundary element procedure. Mysore et al. [108] used a finite element method to model an inflatable dam structure, and a boundary element technique to determine the behavior of the fluid. Ergin et al. [109] studied the dynamic behavior of a thin, horizontal cylindrical shell vibrating at fixed positions below a free surface in water of finite depth. By using a boundary element technique, they calculated the generalized fluid loading to assess the influence of free

surface, rigid boundary and position of submerged cylinder on the dynamic characteristics of the shell structure.

Nestegård and Mejlænder-Larsen [110] proposed a symmetric boundary integral equation method for the fluid flow, coupled with a finite element method for the structure displacements, and presented eigenfrequencies and associated mode shapes of partially submerged three-dimensional structures. More recently, Ergin and Temarel [111] proposed an approach based on a boundary integral equation method and the method of images, in order to calculate the fluid–structure interaction forces of a partially filled and/or submerged horizontal cylindrical shell. In their investigation they calculated the generalized fluid–structure interaction forces in terms of generalized added mass terms, and compared the calculated wet frequencies and mode shapes with experimental data found in the literature.

In this thesis, the dynamic characteristics of fluid storage tanks are investigated using a boundary element method in conjunction with the method of images in order to impose an appropriate boundary condition on the free surface of the fluid. In this investigation, it is assumed that the fluid is ideal, i.e., inviscid, incompressible and its motion is irrotational. Furthermore, the fluid forces are associated with the inertial effect of the fluid, i.e., the fluid pressure on the wetted surface of the structure is in phase with the structural acceleration. In the analysis, it is assumed that the flexible structure vibrates in its *in vacuo* eigenmodes when it is in contact with fluid, and that each mode gives rise to a corresponding surface pressure distribution on the wet part of the structure. The *in*

vacuo dynamic analysis entails the vibration of the elastic structure in the absence of any external force and structural damping.

At the fluid–structure interface, continuity considerations require that the normal velocity of the fluid is equal to that of the structure. The normal velocities on the wetted shell are expressed in terms of modal structural displacements, obtained from the *in vacuo* dynamic analysis. By using the boundary integral equation method the fluid pressure is eliminated from the problem, and using the method of images (i.e., imposing an appropriate free surface boundary condition, namely $\Phi = 0$, here Φ is the deformation potential), the fluid–structure interaction forces are calculated solely in terms of generalized added mass coefficients. During this analysis, the wet surfaces are idealized by using appropriate boundary elements, referred to as hydrodynamic panels. The generalized structural mass matrix is merged with the generalized added mass matrix and then the total generalized mass matrix is used in solving the eigenvalue problem.

Formulation of the Fluid Problem

Suppose the pressure vessel is filled with some kind of fluid. Now we will discuss how the fluid affects the dynamic properties of the vessel. The fluid is assumed ideal, i.e., inviscid and incompressible, and its motion is irrotational and there exists a fluid velocity vector, **v**, which can be defined as the gradient of the velocity potential function Φ as

$$\mathrm{v}(x, y, z, t) = \nabla \Phi(x, y, z, t) \tag{8}$$

where Φ satisfies Laplace's equation

$$\nabla^2\Phi(x,y,z,t)=0 \tag{9}$$

i.e.,

$$\frac{\partial^2\Phi}{\partial x^2}+\frac{\partial^2\Phi}{\partial y^2}+\frac{\partial^2\Phi}{\partial z^2}=0$$

throughout the fluid domain.

For the structure vibrating with frequency ω, the response of the structure may be expressed as $p(t)=p_0e^{i\omega t}$, where p_0 is the vibration amplitude. Thus the velocity potential function Φ_r due to the deformed shape of the structure in the rth modal vibration may be written as ([111])

$$\Phi_r(x,y,z,t)=i\omega\phi_r(x,y,z)p_re^{i\omega t},\quad r=1,2,...,M \tag{10}$$

where ϕ_r is the deformation potential. i is the imaginary unit and ω is the natural circular frequency of vibration. M represents the number of modes of interest, and p_r is the amplitude of the rth modal vibration.

On the wetted surface of the vibrating structure, the fluid normal velocity must be equal to the normal velocity on the structure and this condition can be expressed as

$$-\frac{\partial\phi}{\partial\mathbf{n}}=\mathbf{u}\,.\,\mathbf{n} \tag{11}$$

where **u** is the displacement vector of the median surface of the structure and **n** is the unit normal vector on the wetted surface and points into the region of interest.

In this study, it is assumed that the structure vibrates at relatively high frequencies so that the effect of surface waves, for the partially filled and/or submerged shell, can be neglected. Therefore, the free surface condition for ϕ can be approximated by

$$\phi = 0, \text{ on the free surface} \tag{12}$$

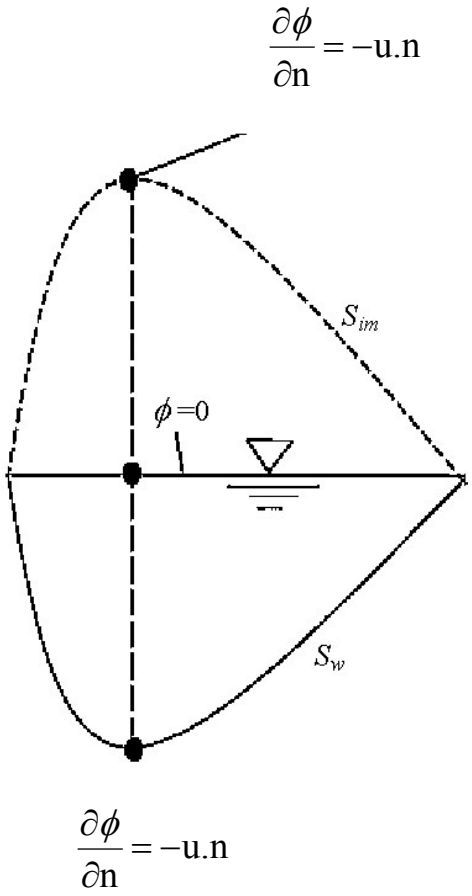

Figure 2. Wetted surface and image boundary for a partially filled structure (from [109])

The method of images [111] may be used, as shown in Fig. 2, to satisfy this condition. By adding an imaginary boundary region, the condition given by Eq. (12) at the horizontal

surface can be omitted; thus the problem is reduced to a classical Neumann case. It should also be noted that the normal fluid velocity cannot be arbitrarily specified. It has to satisfy the incompressibility condition

$$\iint_{Sw+Sim} \frac{\partial \phi}{\partial \mathbf{n}} dS = 0 \tag{13}$$

where S_w and S_{im} represent the wetted and image surfaces respectively (see Fig. 2).

Numerical Evaluation of Deformation Potential ϕ

The deformation potential, ϕ, in a three-dimensional inviscid flow field due to the oscillating elastic structure, can be obtained for only a limited number of cases. An alternative solution method must be employed for a general type of structure and domain.

Green's theorem suggests that, we can use a method that reduces the calculation of ϕ to integration over the boundary surfaces. In the present study, a boundary integral equation method [114, 115] is applied in order to evaluate the fluid-structure interaction forces.

The deformation potential, ϕ, can be expressed by means of a distribution of unknown source strength, σ, over the wetted and image surfaces of the structure [114, 115] in the following form

$$\phi(\mathrm{r}) = \iint_{S_w+S_{im}} \frac{\sigma(\mathrm{r}_0)}{R(\mathrm{r},\mathrm{r}_0)} \mathrm{d}S \tag{14}$$

where

$R=[(x-x_0)^2+(y-y_0)^2+(z-z_0)^2]^{1/2}$,

and $\mathbf{r}=(x,y,z)$ denotes the position vector of the field point within the fluid, $\mathbf{r}_0=(x_0,y_0,z_0)$ is the position vector of a source point on the wetted/image surface of the structure.

Substituting boundary conditions (Eq. (11) and Eq. (12)) into Eq. (14), the unknown strength σ can be determined from the set of algebraic equations

$$2\pi\sigma_i - \sum_{j=1}^{N} \sigma_j \iint_{\Delta s_j} \frac{\partial}{\partial \mathrm{n}} \left[\frac{1}{R(\mathrm{r}_i, \mathrm{r}_j)} \right] dS = u_{ni}, \qquad i = 1,2,...,N. \tag{15}$$

where ΔS_j represents the area of the jth panel, N is the number of panels required to discretize the wetted and image surfaces and u_{ni} denotes the modal displacement in the direction of the normal at the control point (x_i,y_i,z_i) of the ith panel.

Generalized Fluid-structure Interaction Forces

Once the deformation potentials ϕ due to the oscillation of the body in its *in vacuo* eigenmodes are obtained, the kth component of the generalized fluid-structure interaction force amplitude due to the rth modal vibration can be expressed in terms of the pressure acting on the wetted surface of the structure as

$$F_{kr}(t) = \iint_{S_W} P_r(x,y,z,t)\mathrm{n}_k.\mathrm{n}\, dS \tag{16}$$

P_r is the pressure acting on the wetted surface due to the rth modal vibration. $\mathbf{n}_k$ is a unit vector in the direction of the kth component force, and $\mathbf{n}$ is the unit normal vector of the surface.

According to the Bernoulli's equation and neglecting the second order terms, the dynamic fluid pressure on the mean wetted surface of the flexible structure due to the *r*th modal vibration becomes

$$P_r(x,y,z,t) = -\rho \frac{\partial \Phi_r}{\partial t} \tag{17}$$

By substituting Equation (10) into Equation (17), the following expression for the pressure is obtained:

$$P_r(x,y,z,t) = \omega^2 \rho \varphi_r(x,y,z) p_r e^{i\omega t} \tag{18}$$

The *k*th component of the generalized fluid-structure interaction force amplitude due to the *r*th modal vibration then takes the form

$$F_{kr}(t) = \iint_{Sw} P_r(x,y,z,t) \mathrm{n}_k . \mathrm{n}\, dS = p_r e^{i\omega t} \iint_{Sw} \omega^2 \rho \phi_r \mathrm{n}_k . \mathrm{n}\, dS \tag{19}$$

Because the response of the structure can be expressed as $\mathrm{p}(t) = \mathrm{p}_0 e^{i\omega t}$

$$\ddot{p}_r(t) = -\omega^2 p_r e^{i\omega t} \tag{20}$$

The generalized added mass term A_{kr} can be defined as

$$A_{kr} = \rho \iint_{\mathrm{Sw}} \varphi_r \mathrm{n}_\mathrm{k} . \mathrm{n}\, \mathrm{dS} \tag{21}$$

Then according to F=ma,

$$F_{kr}(t) = -A_{kr} \ddot{p}_r(t) \tag{22}$$

So A_{kr} can be seen as the effective mass due to the force of the fluid.

Calculation of Wet Frequencies and Mode Shapes

The generalized equation of motion for the dynamic fluid–structure interaction system assuming free vibrations with no structural damping is

$$[-\omega^2(\mathrm{a}+\mathrm{A})+\mathrm{c}]\mathrm{p}=0 \tag{23}$$

where $\mathbf{a}=\mathbf{D}^{\mathrm{T}}\mathbf{M}\mathbf{D}$ and $\mathbf{c}=\mathbf{D}^{\mathrm{T}}\mathbf{K}\mathbf{D}$ (Eq. 7) denote the generalized structural mass and stiffness matrices, respectively. The matrix $\mathbf{A}$ (A_{kr}) represents the generalized added mass coefficients.

Solving the eigenvalue problem, expressed by Eq. (23), the wet frequencies and associated mode shapes of the elastic structure in contact with fluid are obtained. To each wet frequencies ω_{r}, there is a corresponding wet eigenvector $\mathbf{p}_{\mathrm{or}}=\{p_{r1},p_{r2},\ldots,p_{rm}\}$ satisfying Eq. (23). The corresponding uncoupled mode shapes, $\overline{\mathbf{u}}_r$, for the structure partially or totally in contact with fluid are obtained as

$$\overline{\mathrm{u}}_r(x,y,z)=\{\overline{u}_r,\overline{v}_r,\overline{w}_r\}=\sum_{j=1}^{M}\mathrm{u}_j(x,y,z)\mathrm{p}_{rj} \tag{24}$$

where $\mathbf{u}_j\ (x, y, z)=\{u_j, v_j, w_j\}$ denote the *in vacuo* mode shapes of the elastic structure and M is the number of mode shapes included in the analysis.

Finite Element Analysis of Pressure Vessel

In Vacuo Pressure Vessel

A finite element model was created in NASTRAN to simulate the dynamic characteristics of the PV. The aluminum liner of the tank has a varying thickness. The middle of the tank

has the smallest thickness of 0.12 in. and the thickness increases to the maximum value of 0.37 in. at both openings of the tank. Shell elements with varying thickness were created by the FIELD tool in PATRAN. Separate scalar functions were used to represent the thickness of the wall, dome and end parts. A total of 8208 elements were used.

Firstly, modal analysis was performed on the finite element model for the aluminum liner tank without composite overwrap and without liquid. The first 6 mode shapes are shown in Figure 3. The tank is clamp-free.

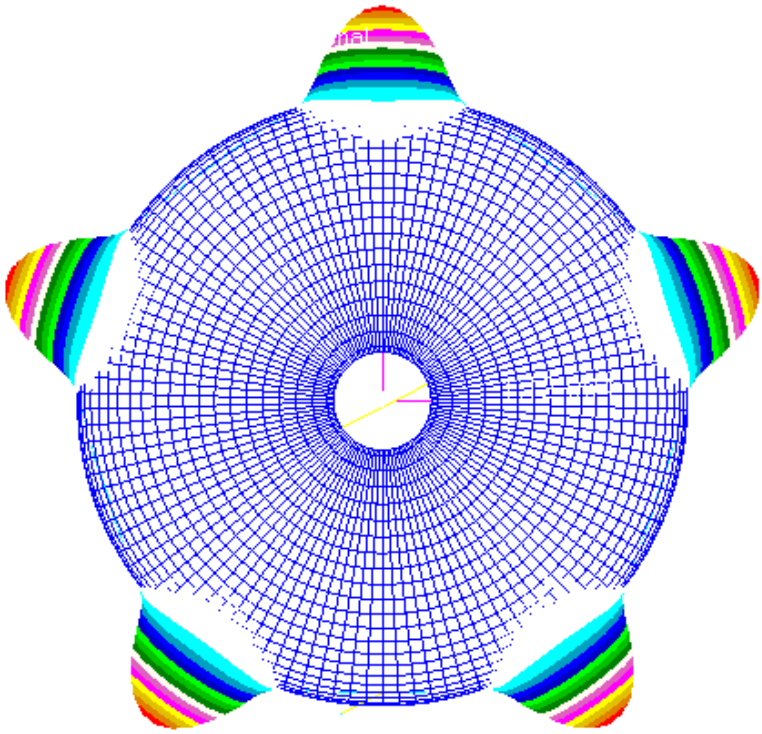

Figure 3(a). Vibration shapes and frequencies of Mode 1 (835 Hz)

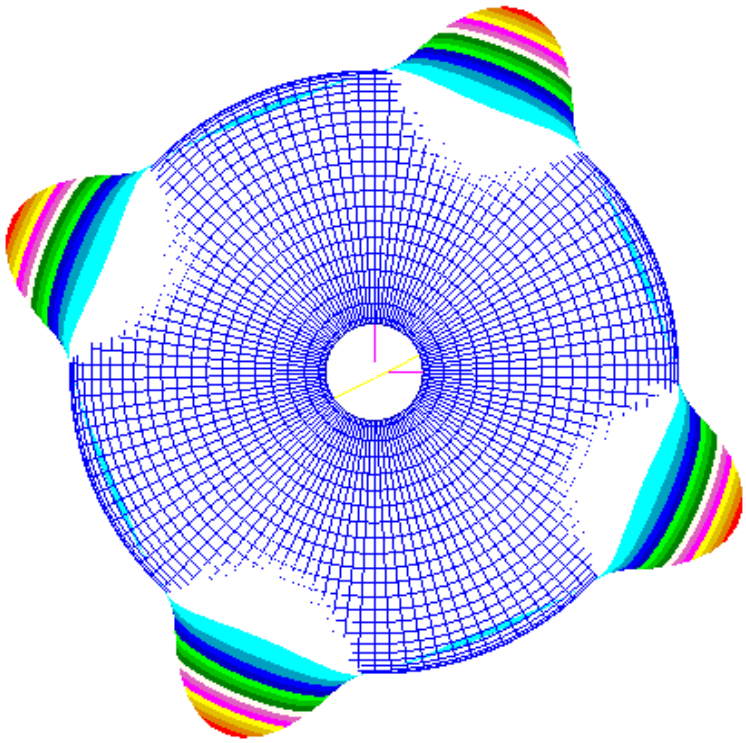

Figure 3(b). Vibration shapes and frequencies of Mode 2 (864 Hz)

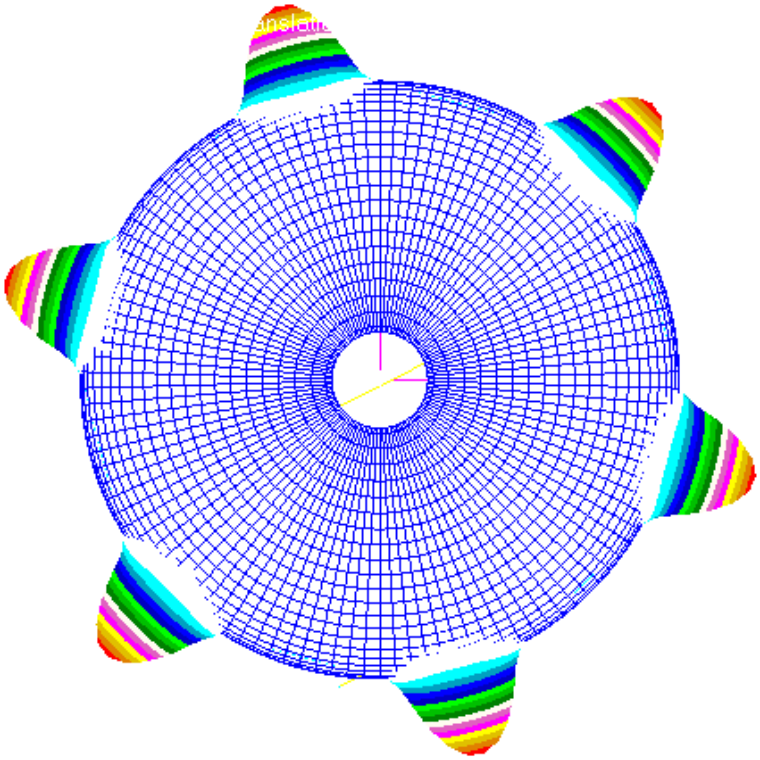

Figure 3(c). Vibration shapes and frequencies of Mode 3 (963 Hz)

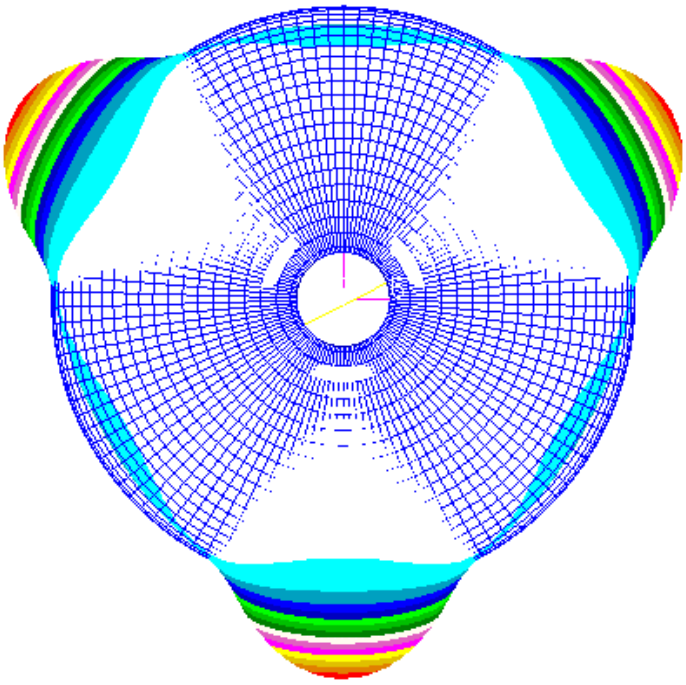

Figure 3(d). Vibration shapes and frequencies of Mode 4 (1090 Hz)

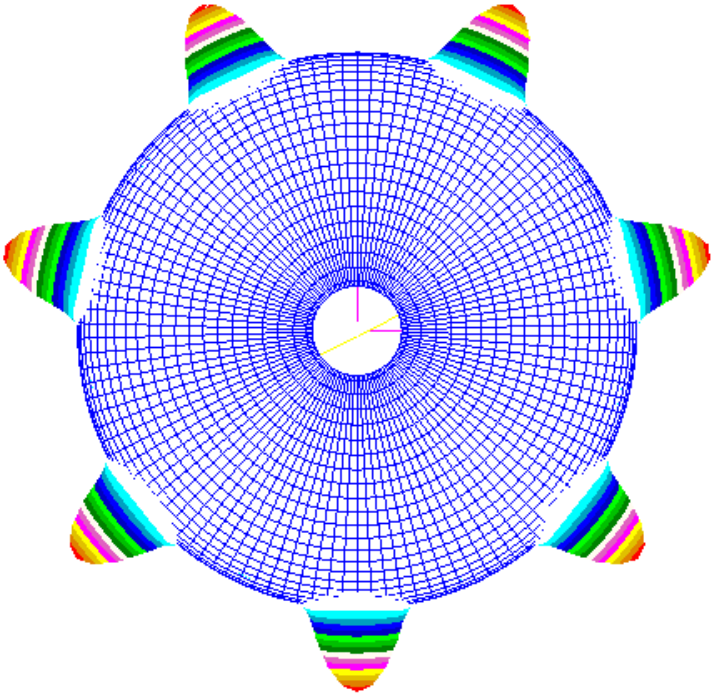

Figure 3(e). Vibration shapes and frequencies of Mode 5 (1199 Hz)

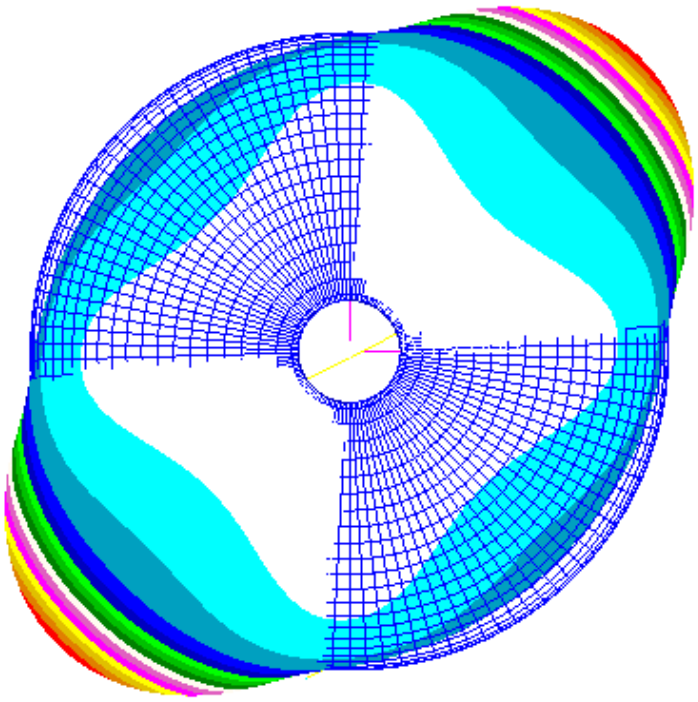

Figure 3(f). Vibration shapes and frequencies of Mode 6 (1518 Hz)

It can be seen that the number of humps in the middle band of the tank for the bending modes does not start from a small number and increase sequentially for the higher order modes as seen in most in most of the dynamic characteristics for regular structures. During the analysis, it is also noted that the natural frequencies are very sensitive to the thickness of the tank.

The Virtual Fluid Mass Method

For the analysis of water-filled tank in NASTRAN, the virtual mass method (MFLUID) based on the above theory was utilized. Nastran doesn't provide many tools for fluid-structure interaction problems. The virtual mass method takes the effect of fluid on a

structure as an added mass when analyzing the dynamic properties of the structure. This method is easy to use and gives reasonable results.

Introduction [116]

1. The virtual mass method allows to model the effect of an incompressible fluid on the structure.
2. The fluid domain may be finite or infinite.
3. Structural surfaces can be wetted on one side only or on both sides.
4. The fluid domain may be composed of several disjoint regions.

Applicability

There are some presumptions about the virtual mass method:

1. Both compressibility and surface waves are ignored. The fluid is considered to be incompressible, inviscid and irrotational.
2. Thus, the frequency range of interest must be
   i. above the frequency range of the sloshing modes.
   ii. below the lowest acoustic frequency.
3. Further restrictions:

   The fluid density within a volume must be constant.

4. On the fluid surfaces, the acoustic pressure is assumed to be zero.

In this analysis, water is used. It meets the requirements of 1 and 3. Our interested frequency range is between that of sloshing modes and acoustic modes. Requirement 4, zero acoustic pressure on the fluid surface, can also be easily met.

User Interface

1. The wetted elements are defined on ELIST bulk data entries.

2. The fluid properties are defined on MFLUID bulk data entries that are selected by MFLUID case control commands.

The ELIST Bulk Data Entry

1	2	3	4	5	6	7	8	9
ELIST	LID	E1	E2	E3	E4	E5	E6	E7
	E8	E9	E10	etc.				

Remarks:

- THRU may be used in fields 3 to 8.
- Positive element identifiers indicate that the fluid is on the side the element normal points to.
- Negative element identifiers indicate that the fluid is on the opposite side.
- Only CTRIA3 and CQUAD4 elements may be referenced.
- LID List Identification Number
- E1 Identification number of a structural element

The MFLUID Bulk Data Entry

1	2	3	4	5	6	7	8	9
MFLUID	SID	CID	ZFS	RHO	ELIST1	ELIST2	PLANE1	PLANE2
	RMAX	FMEXACT						

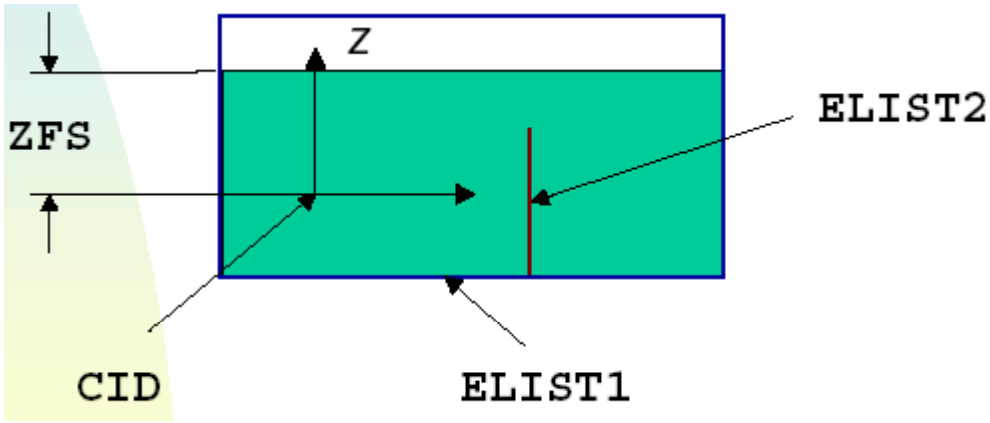

Figure 4. Illustration of MFLUID bulk data entry (from [116]).

The MFLUID Bulk Data Entry

SID Set Identification Number

CID Identification of rectangular coordinate system used to specify the orientation of the free surface and of planes of symmetry

ZFS Position of the free surface (default is infinity)

RHO Density of the fluid

ELIST1 Identification number of an ELIST entry that lists the elements that can be wetted on one side

ELIST2 Identification number of an ELIST entry that lists the elements that can be wetted on both sides

PLANE1, PLANE2 Planes of symmetry (S), antisymmetry (A) or no symmetry (N), no default Plane 1 = *xz*-plane, Plane 2 = *yz*-plane

RMAX Interactions between elements with a distance greater than RMAX will be neglected. (Default: 1.E10)

FMEXACT Exact integration is used if the distance between two elements is

less than FMEXACT times the square root of the area of the larger element. (Default: 1.E15)

Example:

1	2	3	4	5	6	7	8	9
MFLUID	3	2	15.73	1006.0	3	4	S	N

Remarks

First, the dry modes are computed.

Next, the virtual mass matrix is computed and projected onto the dry modes.

Finally, the projected eigenvalue problem is solved providing the wet modes.

Analysis of Tank Filled with Pressurized Water

For the next analysis, the tank is filled with water pressurized at 48 psi. The pressure exerts stiffening effect on the shell. NASTRAN uses the static solution to calculate a differential stiffness matrix that reflects the stiffening effect of the static modes. It then uses that differential stiffness matrix in the modal solution so that different modes are obtained.

Setting up the stiffening effect due to pressure in Nastran is carried out by defining pressure loads on PLOAD2 or PLOAD4 cards. Then include the following types of subcases in Case Control

SUBCASE 1

LABEL = PRESSURE LOAD

LOAD = 1 $ This points to the PLOAD cards

SUBCASE 2

LABEL = MODES

STATSUB=1

METHOD=1 $ This points to the EIGR or EIGRL card

In NASTRAN 2004 the SOL 111 is now capable of accepting a static subcase as an initial condition which takes the effect of differential stiffness to update the modes.

Results for tank completely filled with water are as the following:

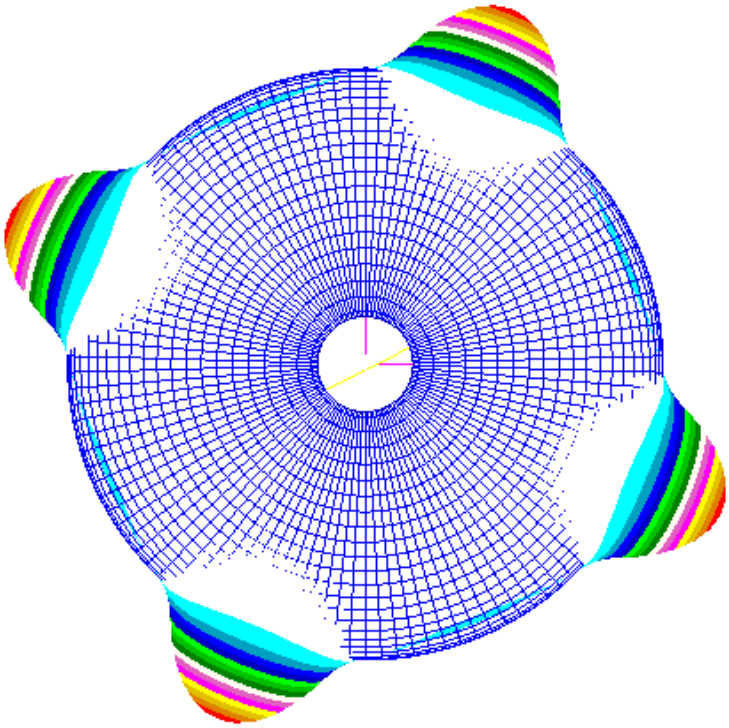

Figure 5(a). Vibration shapes and frequencies of Mode 1
(357 Hz, water), (375 Hz, 48 psi water)

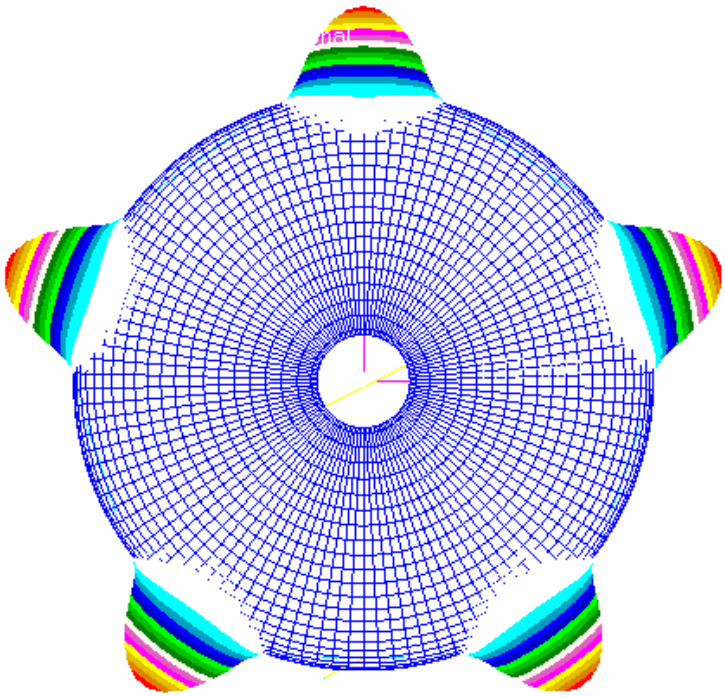

Figure 5(b). Vibration shapes and frequencies of Mode 2 (373 Hz, water), (405 Hz, 48 psi water)

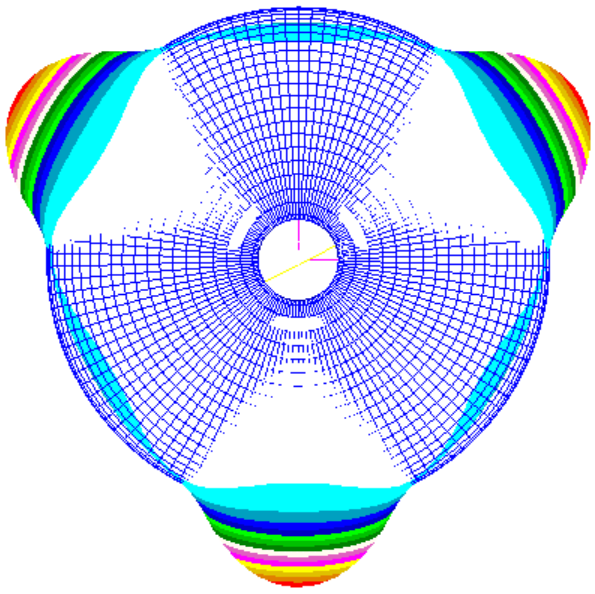

Figure 5(c). Vibration shapes and frequencies of Mode 3 (410 Hz, water), (417 Hz, 48 psi water)

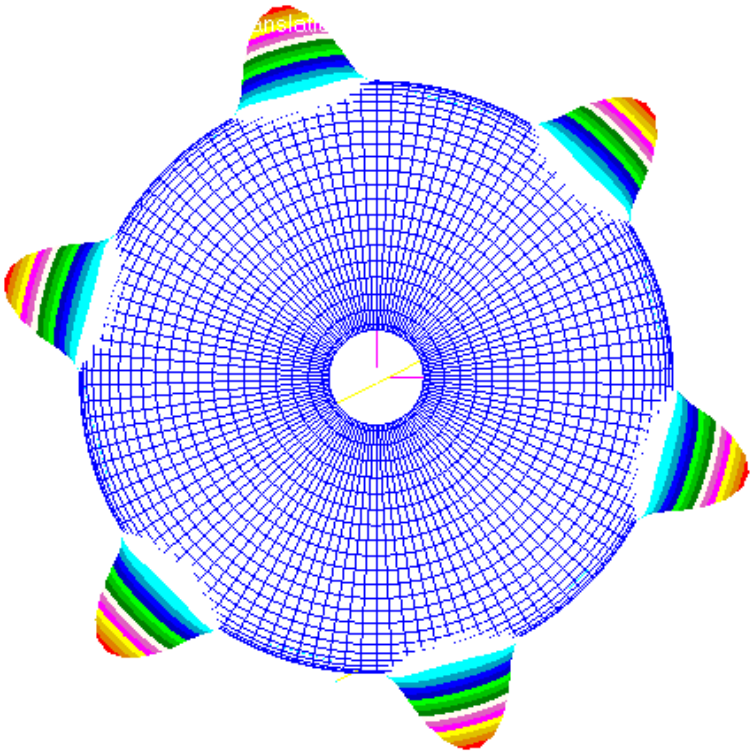

Figure 5(d). Vibration shapes and frequencies of Mode 4 (461 Hz, water), (504 Hz, 48 psi water)

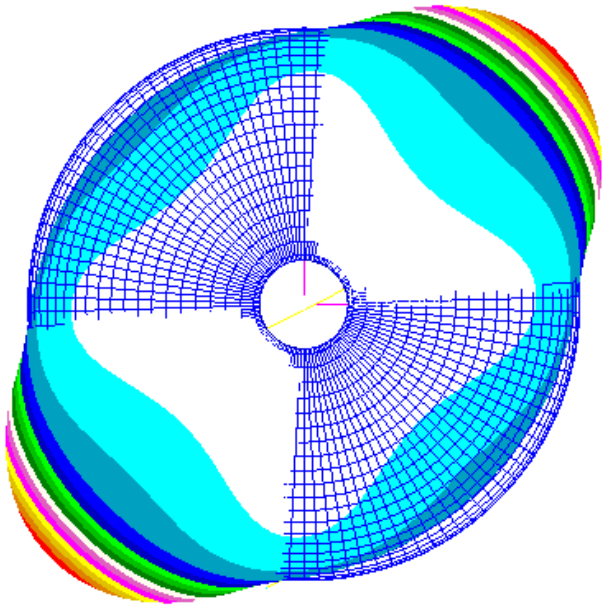

Figure 5(e). Vibration shapes and frequencies of Mode 5 (511 Hz, water), (513 Hz, 48 psi water)

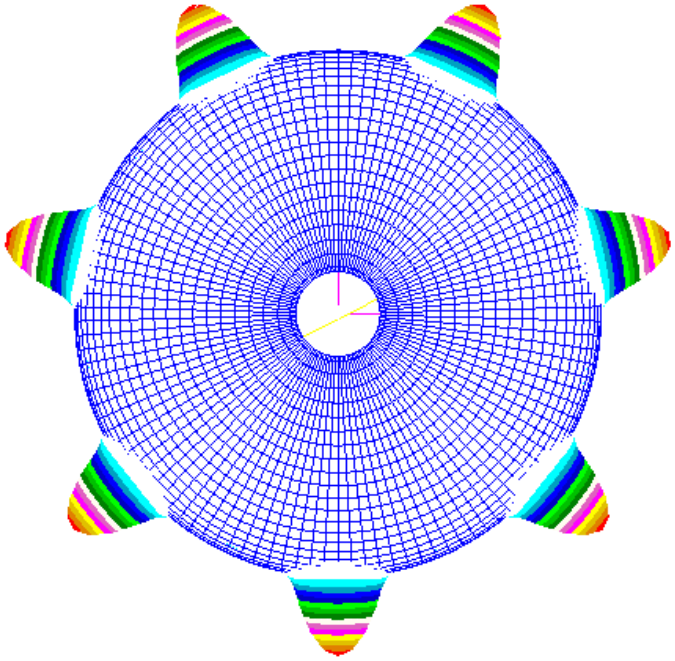

Figure 5(f). Vibration shapes and frequencies of Mode 6 (607 Hz, water), (657 Hz, 48 psi water)

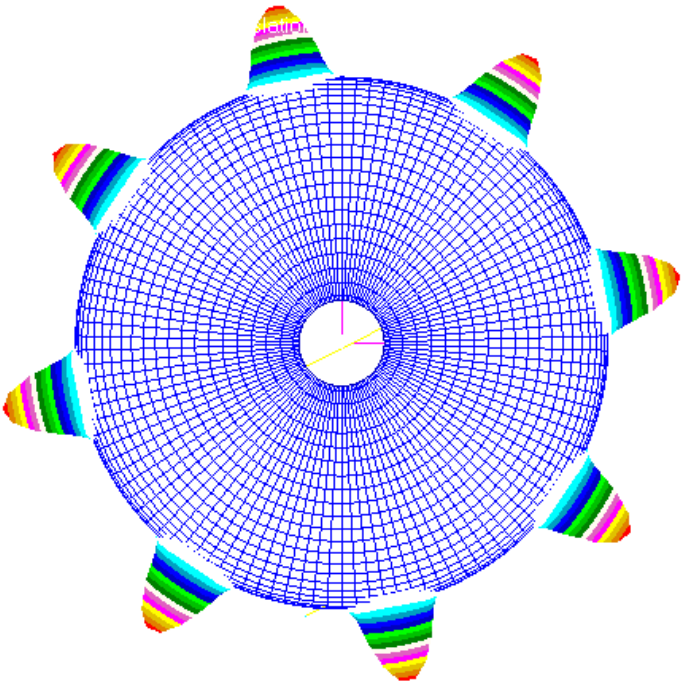

Figure 5(g). Vibration shapes and frequencies of Mode 7 (800 Hz, water), (856 Hz, 48 psi water)

Table 1. Natural frequencies of tank completely filled with water (Hz)

Analysis	Mode1	Mode 2	Mode 3	Mode 4	Mode 5	Mode 6	Mode 7
Water, no pressure	357	373	410	461	511	607	800
Water, 48 psi pressure	375	405	417	504	513	657	856

Remarks:

Compared with the tank *in vacuo*, some modes of the water filled tank are switched in order. Due to the added mass of water, natural frequencies decrease for each mode. For example, the numbers of humps of the first 6 mode shapes from low to high frequencies, for empty tank, are: 5, 4, 6, 3, 7, 2. But for water-filled tank, they are: 4, 5, 3, 6, 2, 7. The natural frequency of mode 1 decreases from 835 Hz to 357 Hz. For mode 2, it decreased from 864 Hz to 373 Hz, etc. Large frequency reduction is observed.

For tank filled with pressurized water, differential stiffness matrix reflecting the stiffening effect is calculated for modal analysis. The natural frequencies increase for each mode, compared with those with no pressure, due to the stiffening effect of pressure. The amounts of increase of frequencies are not very large, and the order of mode shapes keeps the same.

CHAPTER III

DYNAMIC ANALYSIS OF COMPOSITE OVERWRAP PRESSURE VESSEL

For this part, the pressure vessel is over wrapped by 3 hoop layers of carbon fibers, and 2 helical layers. The helical layers make an angle of 40^0 with the hoop layers. Analysis is performed for the dynamic properties (normal modes).

MSC.Nastran uses the assumptions of classical lamination theory in formulating shell behavior for nonuniform and composite laminate element properties. This approach allows the modeling of plates with coupled membrane and bending elastic behavior. This behavior can be simulated directly by entering membrane, bending, membrane-bending coupling and transverse shear constitutive relationships on the PSHELL input or by using the PCOMP entry to define the composite laminate on a ply-by-ply basis.

Classical Lamination Theory

A two-dimensional composite material is defined as a stacked group of laminae arranged to form a flat or curved plate or shell. Each lamina may be considered as a group of unidirectional fibers. The principal material axes for the lamina are parallel and perpendicular to the fiber directions. The principal directions are referred to as "longitudinal" or the 1-direction of the fiber and as "transverse" or the 2-direction for the perpendicular direction (matrix direction).

Classical lamination theory makes the following assumption regarding the behavior of the laminae:

- The laminae are perfectly bonded together.
- The bonds are infinitesimally thin and no lamina can slip relative to another.
- Linear variation of strain through the laminate thickness is assumed.

Deformation in the X-Y plan of the plate at any point C at a distance z in the normal direction to plate middle surface is [117,118]

$$U = U0 + z\,\theta_x \tag{25}$$

$$V = V0 + z\,\theta_y \tag{26}$$

where U, V, and W are the displacements along the X, Y, and Z directions in the element coordinate system, and θ_x, θ_y are the rotations.

The strain-displacement-middle surface strain and curvatures relationship are given by:

$$\begin{Bmatrix} \varepsilon_x \\ \varepsilon_y \\ \gamma_{xy} \end{Bmatrix} = \begin{Bmatrix} \dfrac{\partial U_0}{\partial x} \\ \dfrac{\partial V_0}{\partial y} \\ \dfrac{\partial U_0}{\partial y} + \dfrac{\partial V_0}{\partial x} \end{Bmatrix} + z \begin{Bmatrix} \dfrac{\partial \theta_y}{\partial x} \\ -\dfrac{\partial \theta_x}{\partial y} \\ \dfrac{\partial \theta_y}{\partial y} - \dfrac{\partial \theta_x}{\partial x} \end{Bmatrix} = \begin{Bmatrix} \varepsilon_x^0 \\ \varepsilon_y^0 \\ \gamma_{xy}^0 \end{Bmatrix} - z \begin{Bmatrix} \chi_x \\ \chi_y \\ \chi_{xy} \end{Bmatrix} \tag{27}$$

where the ε^0's and χ's are the middle surface strains and curvatures, respectively.

The stress resultants for an N-layer laminate are obtained by integration of the stresses in each lamina through the laminate thickness as:

$$\begin{Bmatrix} N_x \\ N_y \\ N_{xy} \end{Bmatrix} = \int_{-\frac{t}{2}}^{\frac{t}{2}} \begin{Bmatrix} \sigma_x \\ \sigma_y \\ \tau_{xy} \end{Bmatrix} dz = \sum_{k=1}^{N} \int_{z_{k-1}}^{z_k} \begin{Bmatrix} \sigma_x \\ \sigma_y \\ \tau_{xy} \end{Bmatrix}_k dz \tag{28}$$

$$\begin{Bmatrix} M_x \\ M_y \\ M_{xy} \end{Bmatrix} = -\int_{-\frac{t}{2}}^{\frac{t}{2}} \begin{Bmatrix} \sigma_x \\ \sigma_y \\ \tau_{xy} \end{Bmatrix} z dz = -\sum_{k=1}^{N} \int_{z_{k-1}}^{z_k} \begin{Bmatrix} \sigma_x \\ \sigma_y \\ \tau_{xy} \end{Bmatrix}_k z dz$$

The stress resultant to strain relationship is:

$$\begin{Bmatrix} N_x \\ N_y \\ N_{xy} \end{Bmatrix} = \sum_{k=1}^{N} [G]_k \left\{ \int_{z_{k-1}}^{z_k} \begin{Bmatrix} \varepsilon_x^0 \\ \varepsilon_y^0 \\ \gamma_{xy}^0 \end{Bmatrix}_k dz - \int_{z_{k-1}}^{z_k} \begin{Bmatrix} \chi_x \\ \chi_y \\ \chi_{xy} \end{Bmatrix}_k z dz \right\} \tag{29}$$

$$\begin{Bmatrix} M_x \\ M_y \\ M_{xy} \end{Bmatrix} = \sum_{k=1}^{N} [G]_k \left\{ - \int_{z_{k-1}}^{z_k} \begin{Bmatrix} \varepsilon_x^0 \\ \varepsilon_y^0 \\ \gamma_{xy}^0 \end{Bmatrix}_k z dz + \int_{z_{k-1}}^{z_k} \begin{Bmatrix} \chi_x \\ \chi_y \\ \chi_{xy} \end{Bmatrix}_k z^2 dz \right\} \tag{30}$$

where $[G]_k$ is the material matrix transformed from the laminate coordinate system into the lamina coordinate system.

These relations can be written in the following form used to describe composite elements:

$$\begin{Bmatrix} F \\ M \end{Bmatrix} = \begin{bmatrix} A & B \\ B & D \end{bmatrix} \begin{Bmatrix} \varepsilon^0 \\ \chi \end{Bmatrix} \tag{31}$$

where:

$$[A] = \sum_{k=1}^{N} [G]_k (z_k - z_{k-1})$$

$$[B] = \frac{1}{2} \sum_{k=1}^{N} [G]_k (z_k^2 - z_{k-1}^2)$$

$$[D] = \frac{1}{3} \sum_{k=1}^{N} [G]_k (z_k^3 - z_{k-1}^3)$$

are named in composite element literature as the membrane, membrane-coupling, and bending matrices, respectively.

In the shell element formulation in Nastran, these relationships take the following form:

$$\begin{Bmatrix} F \\ M \\ Q \end{Bmatrix} = \begin{bmatrix} TG_1 & T^2G_4 & 0 \\ T^2G_4 & \frac{T^3}{12}G_2 & 0 \\ 0 & 0 & T_sG_3 \end{bmatrix} \begin{Bmatrix} \varepsilon^0 \\ \chi \\ \gamma \end{Bmatrix} \tag{32}$$

where:

$$[A] = TG_1$$

$$[B] = -T^2G_4$$

$$[D] = \frac{T^3}{12} G_2$$

$$\{Q\} = \begin{Bmatrix} Q_x \\ Q_y \end{Bmatrix} = \text{transverse shear resultants}$$

$$\{\gamma\} = \begin{Bmatrix} \gamma_x \\ \gamma_y \end{Bmatrix} = \text{transverse shear strains}$$

T = nominal plate thickness

T_s = effective transverse shear material thickness

G_1 = membrane matrix

G_2 = bending matrix

G_3 = effective transverse shear matrix

G_4 = membrane-bending coupling matrix

MSC.Nastran allows *G*1, *G*2, *G*4, *T, G*3 and *Ts* to be input directly in PSHELL or to have the composite equivalent material matrices calculated internally from the PCOMP data.

The terms *G*1, *G*2, and *G*4 are defined by the following integrals:

$$G_1 = \frac{1}{T}\int [G_e]dz$$
$$G_2 = \frac{1}{I}\int z^2 [G_e]dz \tag{33}$$
$$G_4 = \frac{1}{T^2}\int (-z)[G_e]dz$$

The limits on the integration are from the bottom surface to the top surface of the laminated composite. The matrix of material moduli, $[G_e]$, has the following form for isotropic materials:

$$[G_e]_i = \begin{bmatrix} \frac{E}{1-\nu^2} & \frac{\nu E}{1-\nu^2} & 0 \\ \frac{\nu E}{1-\nu^2} & \frac{E}{1-\nu^2} & 0 \\ 0 & 0 & \frac{E}{2(1+\nu)} \end{bmatrix} \tag{34}$$

For orthotropic materials, the matrix, $[G_e]$, is written as follows:

$$[G_e]_0 = \begin{bmatrix} \dfrac{E_1}{1-\nu_1\nu_2} & \dfrac{\nu_1 E_2}{1-\nu_1\nu_2} & 0 \\ \dfrac{\nu_2 E_1}{1-\nu_1\nu_2} & \dfrac{E_2}{1-\nu_1\nu_2} & 0 \\ 0 & 0 & G_{12} \end{bmatrix} \tag{35}$$

Here, $\nu_1 E_2 = \nu_2 E_1$ in order to satisfy the requirement that the matrix of elastic moduli be symmetric. In general, the user may supply element properties with respect to a particular orientation which does not necessarily correspond to the principal material axes. In this case, the user must also supply the value of the angle, or material coordinate system that orients the element material axis relative to the side G1-G2 of the element. The material elastic modulus matrix is then transformed by the program into the element modulus matrix through the relation

$$[G_e] = [U]^t [G_m] [U] \tag{36}$$

where:

$$[U] = \begin{bmatrix} \cos^2\theta & \sin^2\theta & \cos\theta\sin\theta \\ \sin^2\theta & \cos^2\theta & -\cos\theta\sin\theta \\ -2\cos\theta\sin\theta & 2\cos\theta\sin\theta & \cos^2\theta - \sin^2\theta \end{bmatrix}$$

The finite element model for a structure composed of composite materials requires the evaluation of the matrix of elastic moduli for each plate element of the model. The characteristics of the composite media are totally contained in these matrices.

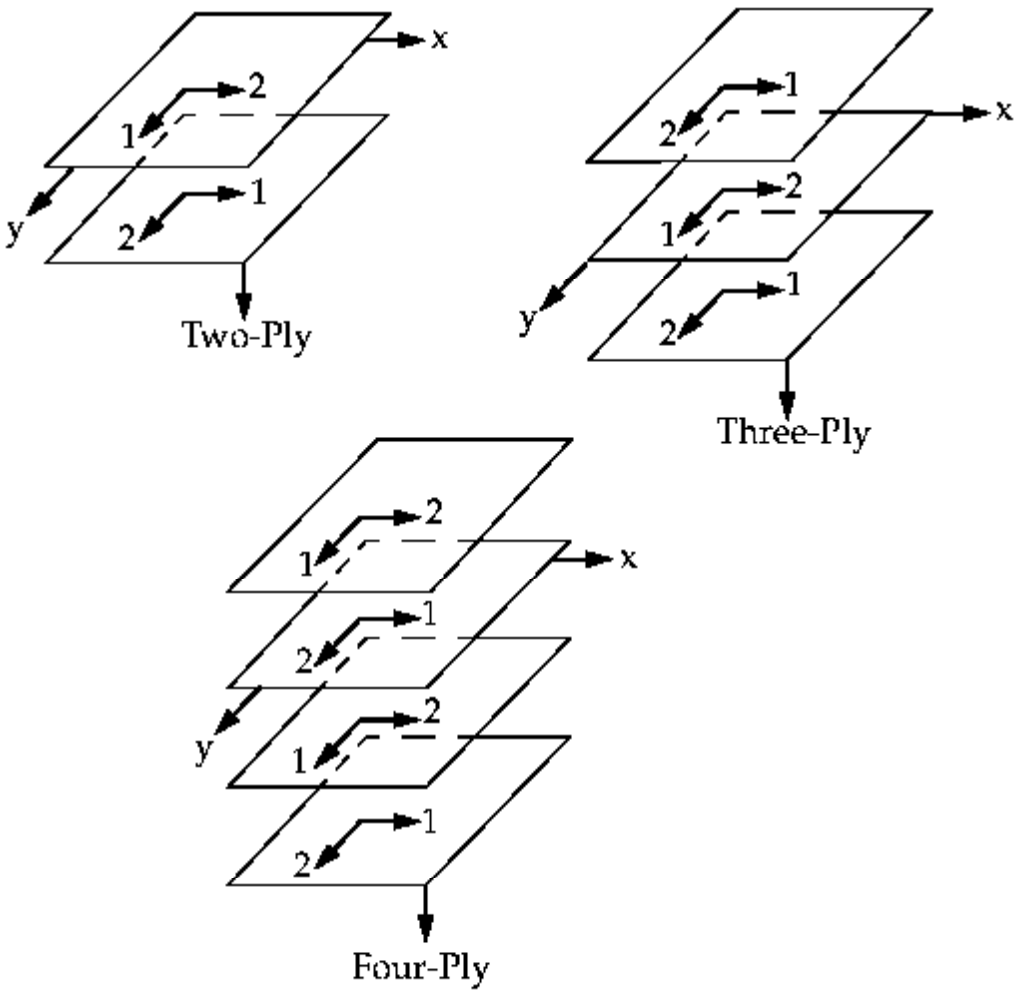

Figure 6 Exploded View of Three Cross-Ply Laminated Plates (from [117]).

To illustrate the evaluation of these matrices, consider the cross-ply laminates of Figure 6. In this portion of the discussion, the three configurations shown in Figure 6 are each assumed to be represented by a single quadrilateral plate element and the coordinate axes

shown are coincident with the element coordinate axes. Then, if it is assumed that each lamina of the n-ply laminates is of thickness *T/n*, where *T* is the total thickness of each of three configurations, the matrices of elastic moduli may be evaluated from the following relations:

$$[G_1] = \frac{1}{T}\left\{ \int_{-\frac{T}{2}}^{-\frac{T}{2}+\frac{T}{n}} [G_e]_1 z^2 dz + \int_{-\frac{T}{2}+\frac{T}{n}}^{-\frac{T}{2}+\frac{2T}{n}} [G_e]_2 dz + \ldots + \int_{-\frac{T}{2}+\frac{(n-1)T}{n}}^{\frac{T}{2}} [G_e]_n dz \right\} \tag{37}$$

$$[G_2] = \frac{1}{T}\left\{ \int_{-\frac{T}{2}}^{-\frac{T}{2}+\frac{T}{n}} [G_e]_1 dz + \int_{-\frac{T}{2}+\frac{T}{n}}^{-\frac{T}{2}+\frac{2T}{n}} [G_e]_2 z^2 dz + \ldots + \int_{-\frac{T}{2}+\frac{(n-1)T}{n}}^{\frac{T}{2}} [G_e]_n z^2 dz \right\} \tag{38}$$

$$[G_4] = \frac{1}{T^2}\left\{ \int_{-\frac{T}{2}}^{-\frac{T}{2}+\frac{T}{n}} [G_e]_1 (-z) dz + \int_{-\frac{T}{2}+\frac{T}{n}}^{-\frac{T}{2}+\frac{2T}{n}} [G_e]_2 (-z) dz + \ldots + \int_{-\frac{T}{2}+\frac{(n-1)T}{n}}^{\frac{T}{2}} [G_e]_n (-z) dz \right\} \tag{39}$$

These relations reflect the assumption that the *xy*-plane of the element coordinate system is coincident with the geometric middle plane of the laminate. The *xy*-plane of the element coordinate system is defined in the mean plane of the element so that any offset between the mean plane of the connected grid points and the geometric middle plane of the laminate would be reflected in the integration limits of the preceding relations.

The matrix of elastic moduli for transverse shear, $[G_3]_m$ is defined as a two-by-two matrix of the form

$$[G_3]_m = \begin{bmatrix} G_{11} & G_{12} \\ G_{21} & G_{22} \end{bmatrix} \tag{40}$$

and the corresponding matrix transformed into an element coordinate system is given by

$$[G_3]_e = [W]^T [G_3]_m [W] \tag{41}$$

where $[W] = \begin{bmatrix} \cos\theta & \sin\theta \\ -\sin\theta & \cos\theta \end{bmatrix}$

The mean value of the transverse shear modulus $\overline{G}$ for the laminated composite is defined in terms of the transverse shear strain energy, U, through the depth

$$U = \frac{1}{2}\frac{V^2}{\overline{G}T} = \frac{1}{2}\int \frac{(\tau(z))^2}{G(z)} dz \tag{42}$$

A unique mean value of the transverse shear strain is assumed to exist for both *x* and *y* components of the element coordinate system, but for ease of discussion, only the evaluation of an uncoupled *x* component of the shear moduli will be illustrated here.

From equation (42) the mean value of transverse shear modulus may be written in the following form

$$\frac{1}{G_x} = \frac{T}{V_x^2} \sum_{i=1}^{N} \int_{z_{i-1}}^{z_i} \frac{(\tau_{zx}(z))^2}{(G_x)_i} dz \tag{43}$$

where G is an "average" transverse shear coefficient used by the element code and $(G_x)_i$ is the local shear coefficient for layer i. To evaluate equation (35), it is necessary to obtain an expression for $(\tau_{zx}(z))$. This can be accomplished by assuming that the x- and y-components of stress are decoupled from one another. This assumption allows the desired equation to be deduced through an examination of a beam unit cross-sectional width.

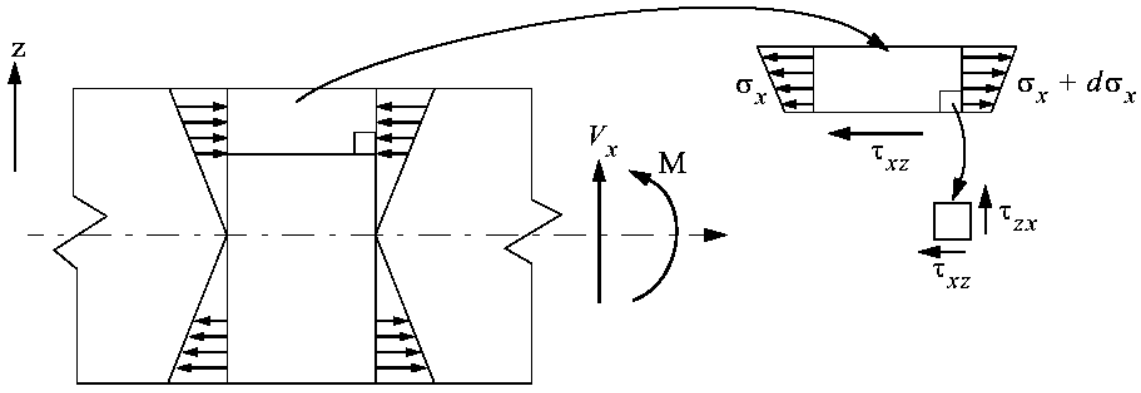

Figure 7 Illustration of forces and moments acting on composite plies (from [117])

The equilibrium conditions in the horizontal direction and for total moment are

$$\frac{\partial \tau_{xz}}{\partial z} + \frac{\partial \sigma_x}{\partial x} = 0 \tag{44}$$

$$V_x + \frac{\partial M_x}{\partial x} = 0 \tag{45}$$

Now, if the location of the neutral surface is denoted by $\bar{z}_x$ and ρ is the radius of curvature of the beam, the axial stress E_x may be expressed in the form

$$\sigma_x + \frac{E_x(\bar{z}_x - z)}{(\overline{EI})_x} = 0 \tag{46}$$

Equation (46) may be differentiated with respect to *x* combined with Equation (44) and Equation (45). In a region of constant E_x the result may be integrated to yield the following expression

$$\tau_{xz} = C_i + \frac{V_x}{(\overline{EI})_x}(\bar{z}_x z - \frac{z^2}{2})E_{xi} \qquad z_{i-1} < z < z_i \tag{47}$$

Equation (47) is particularly convenient to use in the analysis of n-ply laminates because sufficient conditions exist to determine the constants C*i* (*i* = 1,2,...,n) and the "directional bending center" $\bar{z}_x$. For example, consider the following laminated configuration

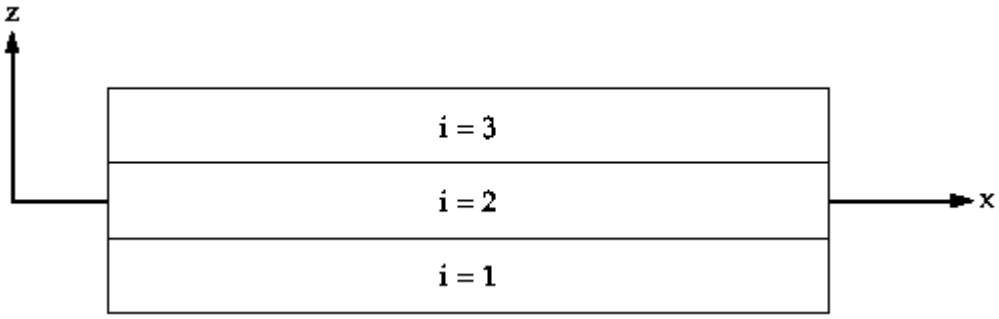

Figure 8. A laminated configuration of three plies

At the bottom surface (i=1, z=z_0, and τ_{xz}=0)

$$C_1 = \frac{-V_x}{(\overline{\overline{EI}})_x}(\bar{z}_x z_0 - \frac{{z_0}^2}{2})E_{x1} \tag{48}$$

and for the first ply at the interface between plies $i = 1$ and $i = 2$ ($z = z_1$)

$$(\tau_{xz})_1 = +\frac{V_x}{(\overline{\overline{EI}})_x}\left[\bar{z}_x(z_1 - z_0)\frac{1}{2}[z_1^2 - z_0^2]\right]E_{x1} \tag{49}$$

At this interface between plies $i = 1$ and $i = 2$,

$$(\tau_{xz})_2 = C_2 + \frac{V_x}{(\overline{\overline{EI}})_x}\left(\bar{z}_x z_1 - \frac{z_1^2}{2}\right)E_{x2} \tag{50}$$

and as $(\tau_{xz})_2 = (\tau_{xz})_1$ at $z = z_1$,

$$C_2 = (\tau_{xz})_1 - \frac{V_x E_{x2}}{(\overline{EI})_x}\left(\bar{z}_x z_1 - \frac{z_1^2}{2}\right) \tag{51}$$

Then, in the ply $z_1 < z < z_2$ the shear is

$$\tau_{xz}(z) = (\tau_{xz})_1 \frac{V_x E_{x2}}{(\overline{EI})_x}\left[\bar{z}_x (z - z_1) - \frac{1}{2}(z^2 - z_1^2)\right] \tag{52}$$

In general, for any ply, $z_{i-1} < z < z_i$, the shear is

$$\tau_{xz}(z) = (\tau_{xz})_{i-1} \frac{V_x E_{xi}}{(\overline{EI})_x}\left[\bar{z}_x (z - z_{i-1}) - \frac{1}{2}(z^2 - z_{i-1}^2)\right] \tag{53}$$

At any ply interface, z_i, the shear is therefore

$$(\tau_{xz})_i = \frac{V_x}{(\overline{EI})_x} \sum_{j=1}^{i} E_{xj} T_j \left[\bar{z} - \frac{1}{2}(z_j + z_{j-1})\right] \tag{54}$$

where $T_j = z_j - z_{j-1}$

Note that the shear at the top face, $(\tau_{xz})_n$, is zero and therefore

$$(\tau_{xz})_n = \frac{V_x}{(\overline{EI})}\left[\bar{z}_x \sum_{j=1}^{n} E_{xj}T_j - \sum_{j=1}^{n} E_{xj}T_j(z_j + z_{j-1})/2\right] = 0 \tag{55}$$

Equation (55) proves that if z_x is the bending center, the shear at the top surface must be zero.

Equation (53) could be substituted into equation (44) and integrated. A better form of equation (55), for this purpose is

$$(\tau_{xz}(z))_i = \frac{V_x E_{xi}}{(\overline{EI})_x}\left[f_{xi} + \bar{z}_x(z - z_{i-1})\frac{1}{2}(z^2 - z_{i-1}^2)\right] \tag{56}$$

where

$$f_{xi} = \frac{1}{E_{xi}} \sum_{j=1}^{i-1} E_{xj}T_j\left[\bar{z}_x - \frac{1}{2}(z_j + z_{j-1})\right] \tag{57}$$

Substituting Equation (56) into Equation (57) and after a considerable effort of integrating the results, we obtain

$$\frac{1}{G_x} = \frac{T}{(\overline{EI})_x^2} \sum_{i=1}^{N} \frac{1}{G_{xi}} R_{xi} \tag{58}$$

where

$$R_{xi} = (E_{xi})^2 T_i \left[\left\{ f_{xi} + (\bar{z}_x - z_{i-1}) T_i - \frac{1}{3} T_i^2 \right\} f_{xi} \right.$$
$$\left. + \left\{ \frac{1}{3}(\bar{z}_x - 2z_{i-1}) - \frac{1}{4} T_i \right\} \bar{z}_x T_i^2 + \left\{ \frac{1}{3} z_{i-1}^2 + \frac{1}{4} z_{i-1} T_i + \frac{1}{20} T_i^2 \right\} T_i^2 \right] \tag{59}$$

This expression for the inverse shear modulus for the *x*-direction may be generalized to provide for the calculation of each term in the two-by-two matrix of shear moduli.

$$[\overline{G}_{kl}] = \left[\frac{T}{(\overline{EI})_{kk}^2} \sum_{i=1}^{n} [G_{kl}^i]^{-1} R_{ki} \right]^{-1} \tag{60}$$

where

$k = 1,2$

$l = 1,2$

Note that if no shear is given, $[G^i]^{-1} = 0$.

The moduli for individual plies are provided through user input because, in general, $G_{12} \neq G_{21}$, will be used for the coupling terms. Finally,

$$[G_3] = \begin{bmatrix} \overline{G}_{11} & (\overline{G}_{12})_{\text{avg}} \\ (\overline{G}_{12})_{\text{avg}} & \overline{G}_{22} \end{bmatrix} \tag{61}$$

Modeling Composite Overwrap Pressure Vessel (COPV) Using PCOMP

The pressure vessel is over wrapped by 3 layers of carbon fibers in the hoop direction, and 2 layers in the helical direction. The helical layers make an angle of 40^0 with the hoop layers.

The PCOMP command in NASTRAN is used for the dynamic analysis of the COPV.

The Composite Element (PCOMP)

PCOMP provides a property definition specifically for performing composite analysis. PCOMP uses the material properties for each of the lamina to calculate and treat the laminate as an equivalent shell of anisotropic materials.

The format of the PCOMP Bulk Data entry is as follows:

Table 2. Entries of PCOMP

PCOMP	PID	Z0	NSM	SB	FT	TREF	GE	LAM
	MID1	T1	THETA1	SOUT1	MID2	T2	THETA2	SOUT2
	MID3	T3	THETA3	SOUT3	Etc.			

Field **Contents**

PID Property identification number.

Z0 Distance from the reference plane to the bottom surface.

NSM	Nonstructural mass per unit area.
SB	Allowable shear stress of the bonding material.
FT	Failure theory.
TREF	Reference temperature.
LAM	“Blank”, “SYM”, “MEM”, “BEND” option.
MIDi	Material ID of the various plies. The plies are identified by serially numbering them from 1 at the bottom layer.
Ti	Thicknesses of the various plies.
THETAi	Orientation angle of the longitudinal direction of each ply with the material axis of the element.
SOUTi	Stress or strain output request.

Each lamina can be modeled as an isotropic material (MAT1), two-dimensional anisotropic material (MAT2), or orthotropic material (MAT8).

For this COPV model, The PCOMP has six layers, one for the aluminum skin and one for each layer of composite fibers. The entries are organized as the following for the main part of the vessel:

```
PCOMP   2               0.
        1   0.128               2   0.005   90.
        2   0.005   50.         2   0.005   90.
        2   0.005   -50.        2   0.005   90.
```

The case of COPV filled with water is analyzed in the similar fashion.

Theoretical Description

MSC.Nastran develops mass and stiffness data from PCOMP input in a two-step process. First, the PCOMP input data are considered together with the material data referenced by MIDi entries to produce PSHELL/MAT2 combinations that will lead to the required stiffness results and then this spawned data are used in the actual stiffness and mass calculations. The spawned PSHELL has four MIDis, identifying the MAT2s to be used for membrane, bending, transverse shear and membrane-bending coupling.

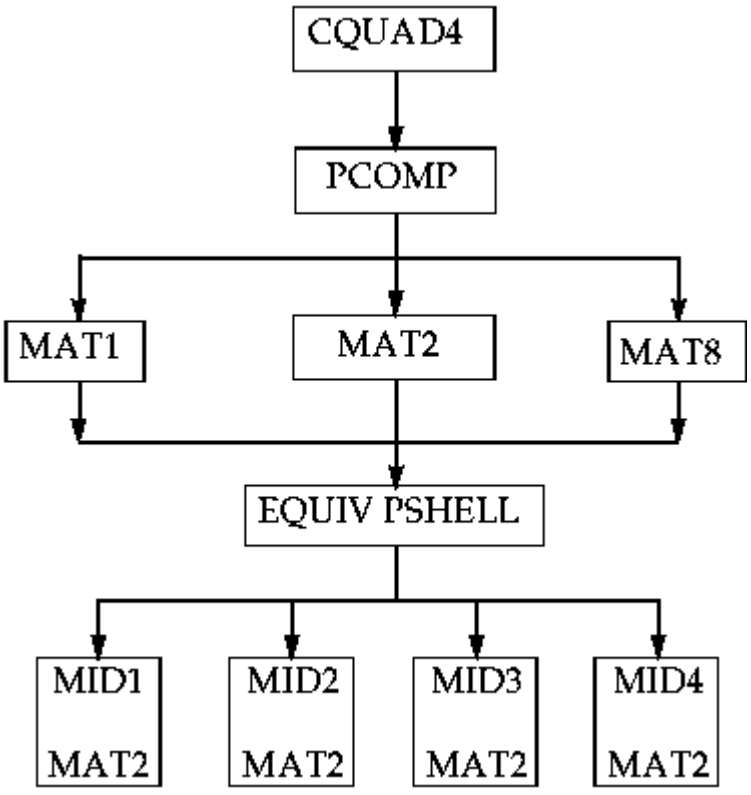

Figure 9. Equivalent PSHELL and MAT2 Entries Generation (from [117])

Where

MID1	Material identification number for the membrane.
MID2	Material identification number for bending.
MID3	Material identification number for transverse shear.
MID4	Material identification number for membrane-bending coupling.

One specifies the material properties and orientation for each of the layers and MSC.Nastran produces the equivalent PSHELL and MAT2 (anisotropic material) entries. Additional stress and strain output is generated for each layer and between the layers.

Results

The first 6 modes are as follows:

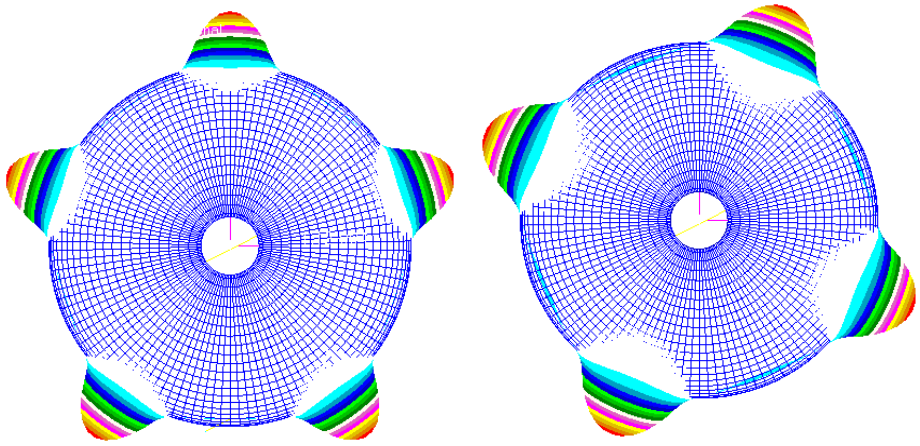

Figure 10(a): Mode shape 1 Figure 10(b): Mode shape 2

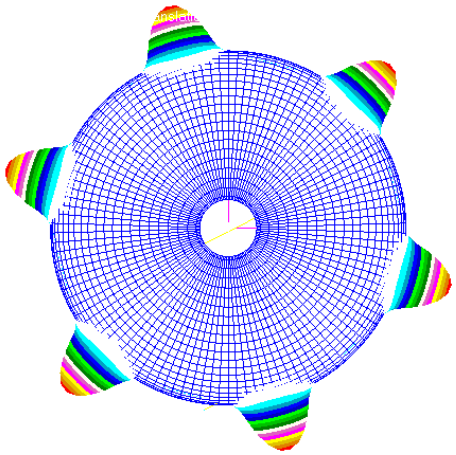

Figure 10(c): Mode shape 3

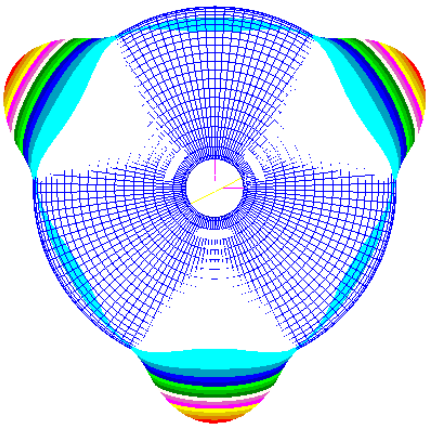

Figure 10(d): Mode shape 4

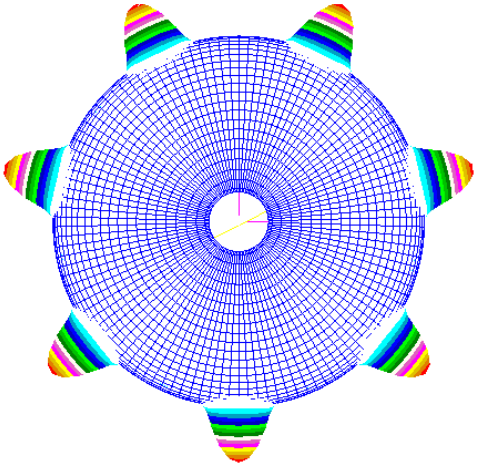

Figure 10(e): Mode shape 5

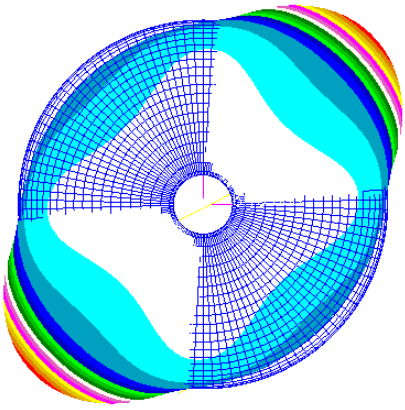

Figure 10(f): Mode shape 6

Table 3. Natural frequencies for tank of aluminum, with overwrap and overwrap, water-filled respectively

Analysis	Mode 1	Mode 2	Mode 3	Mode 4	Mode 5	Mode 6
Aluminum	823	848	955	1069	1193	1493
Overwrap	913	894	1094	1087	1378	1490
Overwrap, water-filled	431	391	552	433	735	529

Remark:

From the above analysis results, it can be seen that, the overall moduli of the composite shell structure increase, compared with the empty aluminum tank, due to the high moduli of the carbon fiber. This leads to the stiffness increase of the tank. Most of the modal frequencies increase, and the orders of some modes are also switched.

CHAPTER IV

CONCLUSIONS

Composite Overwrap Pressure Vessel (COPV) has been widely used in many applications. The composite overwrap increases the pressure carrying capacity of the vessel while keeps the weight light. The composite overwrap is typically in the form of laminates with multiple layers of uni-directional carbon fibers. This class of composite material is not well understood for their properties. To ensure safe operation of the structural system consisting COPV, an on-line automatic structural health monitoring system is needed to constantly monitor the performance of the structure. Many of the health monitoring systems utilize the global or local dynamic characteristics of the structure. The monitoring system can identify the change of dynamic characteristics of the structure, thus detects changes or damages in the structure. In the first part, a review is done on the current progress of health monitoring techniques of composite overwrap pressure vessel.

This thesis studies the dynamic behavior of composite overwrap pressure vessel. Firstly, the dynamic characteristics of the COPV were studied for an empty aluminum tank. Then the tank is completely filled with water, and finally the tank is filled with water at a pressure of 48 psi.

Compared with the tank *in vacuo*, some modes of the water-filled tank are switched in orders. Due to the added mass of water, natural frequencies decrease with each mode.
For tank filled with pressurized water, the pressure exerts a stiffening effect on the tank. The natural frequencies increase with each mode, compared with those with no pressure, due to the stiffening effect of the pressure.

Second, the aluminum tank is overwrapped with uni-directional carbon fiber, and then filled with water both without and with pressure. Due to the high moduli of the carbon fiber overwrapping, the overall moduli of the composite shell structure increase, compared with the empty aluminum tank. This leads to the increase of stiffness of the tank. Most of the modal frequencies increase, and the orders of some modes are also switched, as can be seen from the analysis results.

This research shows that, the dynamic characteristics of the pressure vessel changes at different conditions, and composite overwrap changes the overall dynamic characteristics too, thus making it possible to identify the working conditions and ensure safety operation of the pressure vessel, or a structure. The health monitoring techniques introduced in Chapter I are based on this performance of structures. When proper smart materials such as piezoceramics are used in the health monitoring system, the changes in the dynamic characteristics of a structure are identified by the system. If the structure is not working safely, the health monitoring system may issue warnings or trigger structural control system to bring the structural performance back to normal.

REFERENCES

1. Zou, Y., 2000, "Vibration-based Model Dependant Damage (Delamination) Identification and Health Monitoring for Composite Structures- a Review", *Journal of Sound and Vibration*, 230(2), 357-378

2. Song, Gangbing, Gu, Haichang and Li, Hongnan, 2004, "Application of the Piezoelectric Materials for Health Monitoring in Civil Engineering: An Overview", *Earth and Space 2004: proceedings of the Ninth biennial ASCE Aerospace Division International Conference on Engineering, Construction, and Operations in Challenging Environment.*

3. G. Sun, P. N. Bennett and F. W. Williams, 1997, "An Investigation on Fundamental Frequencies of Laminated Circular Cylinders Given by Shear Deformable Finite Elements", *Journal of Sound and Vibration*, 205(3), 265-273

4. B. Su, Gouri S. Bhuyan, 1998, "Effect of composite wrapping on the fracture behavior of the steel-lined hoop-wrapped cylinders", *International Journal of Pressure Vessels and Piping* 75 (1998), 931–937

5. Y. Kisioglu, J. R. Brevick and G. L. Kinzel, 2001, "Determination of Burst Pressure and Location of the DOT-39 Refrigerant Cylinders", *Journal of Pressure Vessel Technology* 123, 240 (2001).

6. Hill, E. K., Walker, J. L., and Rowell, G. H., 1996, "Burst Pressure Prediction in Graphite/Epoxy Pressure Vessels Using Neural Networks and Acoustic Emission Amplitude Data", *Materials Evaluations*, June.

7. Sun, X. K., Du, S. Y., and Wang, G. D., 1999, "Bursting Problem of Filament Composite Pressure Vessels", *Int. J. Pressure Vessels Piping*, **76**, pp: 55–59.

8. Tadmor, E. B., and Durban, D., 1995, "Plastic Deformation and Burst of Pressurized Multilayered Cylinders", *ASME J. Pressure Vessel Technol*., **117**, Feb., pp. 85–91.

9. Blandford, G. E., Tauchert, T. R., and Leigh, D. C., 1989, "Nonlinear Analysis of Axisymmetric Layered Pressure Vessels—Part 1: Theory", *ASME J. Pressure Vessel Technol.*, **111**, May, pp. 113–119

10. Updike, D. P., and Kalnins, A., 1998, "Tensile Plastic Instability of Axisymmetric Pressure Vessels", *ASME J. Pressure Vessel Technol*., **1-0**, Feb., pp. 6–11

11. M. Xia, H. Takayanagi and K. Kemmochi, 2001, "Analysis of multi-layered filament-wound composite pipes under internal pressure", *Composite Structures*, Volume 53, Issue 4, September, Pages 483-491

12. R.L. Conder and N.L.Newhouse, Dec. 1980, “Cyclic Pressure Test of a Filament-wound vessel containing liquid nitrogen”, *Cryogenics*, V20

13. Tae-Kyung Hwang, Chang-Sun Hong and Chun-Gon Kim, 2003, “Probabilistic Deformation and Strength Prediction for a Filament Wound Pressure Vessel”, *Composites*: Part B 34 (2003) 481–497

14. Shekhar Kamat, Xiaofeng Su, Alpha Star Corp., “Filament Winding Simulation of a Composite Overwrapped Pressure Vessel”, *46th International SAMPE Symposium*

15. M. Amabili and G. Dalpiza, 1995, “Breathing vibrations of a horizontal circular cylindrical tank shell, partially filled with liquid”, Transactions of the American Society of Mechanical Engineers, *Journal of Vibration and Acoustics* 117, 187-191.

16. N. C. Pal, S. K. Bhattacharyya and P. K Sinha, 2003, “Non-linear Coupled Slosh Dynamics of Liquid-filled Laminated Composite Containers: a Two Dimensional Finite Element Approach”, *Journal of Sound and Vibration* Volume 261, Issue 4, 3 April, Pages 729-749

17. M. Amabili, F. Pagnanelli & M. Pellegrini, “Experimental Modal Analysis of a Water-filled Circular Cylindrical Tank”, *Fluid Structure Interaction*, pp. 267-276, WIT press, 2001

18. M. Amabili, F, 1998, “Nonlinear Vibration of Simply Supported, Circular Cylindrical Shells, Coupled to Quiescent Fluid”, *Journal of Fluids and Structures* (1998) 12, 883–918

19. M. Amabili, R. Garziera & F. Pagnanelli, 2001, “Comparison of Theoretical and Experimental Results for Large-amplitude Vibrations of Fluid-filled, Circular Cylindrical Shells”, *Fluid Structure Interaction*, WIT press, page 119-128

20. Amabili M., 1996, “Free Vibration of Partially Filled, Horizontal Cylindrical Shells”, *Journal of Sound and Vibration* Volume 191, Issue 5, 18 April, Pages 757-780

21. S. P. Singh and K. Gupta, 1994, “Damped Free Vibrations of Layered Composite Cylindrical Shells”, *Journal of Sound and Vibration* 2 , 28 April 1994, Pages 191-209

22. D. A. Saravanos, 1999, “Damped Vibration of Composite Plates with Passive Piezoelectric-resistor Elements”, *Journal of Sound and Vibration* Volume 221, Issue 5, 15 April 1999, Pages 867-885

23. T. Maeda, V. Baburaj, Y. Ito and T. Koga, 1998, “Flexural–Torsional Coupling Effect on Vibrational Characteristics of Angle-ply Laminates”, *Journal of Sound and Vibration* Volume 210, Issue 3, 26 February 1998, Pages 351-365

24. Ravikiran Kadoli and N. Ganesan, 2004, “Studies on Dynamic Behavior of Composite and Isotropic Cylindrical Shells with PZT Layers under Axisymmetric Temperature Variation”, *Journal of Sound and Vibration* Volume 271, Issues 122, 22 March 2004, Pages 103-130

25. P. K. Parhi, S. K. Bhattacharyya and P. K. Sinha, 2001, “Hygrothermal Effects on the Dynamic Behavior of Multiple Delaminated Composite Plates and Shells", *Journal of Sound and Vibration* Volume 248, Issue 2, 22 November 2001, Pages 195-214

26. S. Rajaa, P. K. Sinha, G. Prathapc and D. Dwarakanathan, 2004, “Influence of Active Stiffening on Dynamic Behavior of Piezo-hygro-thermo-elastic Composite Plates and Shells”, *Journal of Sound and Vibration* Article in Press, Corrected Proof

27. D. T. Detwiler, M. -H. H. Shen and V. B. Venkayya, 1995, "Finite Element Analysis of Laminated Composite Structures Containing Distributed Piezoelectric Actuators and Sensors", *Finite Elements in Analysis and Design* Volume 20, Issue 2, June 1995, Pages 87-100

28. Saravanos D. A. and Hopkins D. A., 1996, “Effects of Delaminations on the Damped Dynamic Characteristics of Composite Laminates: Analysis and Experiments”, *Journal of Sound and Vibration* Volume 192, Issue 5, 23 May 1996, Pages 977-993

29. J. J. Tracy and G. C. Pardoen, 1989, “Effect of Delamination on the Natural Frequencies of Composite Laminates”, *Journal of Composite Materials* 23, 1200-1215.

30. G.L. Nagesh Babu and S. Hanaguid, 1990, “Delaminations in Smart Composite Structures: a Parametric Study on Vibrations”, *31st AIAA/ASME/ASCE/AHS/ASC SDM Conference*, AIAA Paper 90-1173-CP, 2417-2426.

31. A.Paolozzi and I. Peroni, 1990, “Detection of Debonding Damage in a Composite Plate through Natural Frequency Variations”, *Journal of Reinforced Plastics and Composites* 9, 369-389.

32. M. H. H. Shen and J. E. Grady, 1992, “Free Vibrations of Delaminated Beams”, *American Institute of Aeronautics and Astronautics* 30(5), 1361-1370.

33. L. H. Tenek, E. G. Henneke II and M. D. Gunzburger, 1993, “Vibration of Delaminated Composite Plates and Some Applications to Non-destructive Testing”, *Composite Structures* 23, 253-262.

34. J. S. Anastasiadis and G. J. Simitses, 1991, “Spring Simulated Delamination of Axially-loaded Flat Laminates”, *Composite Structures*, 17, 67-85.

35. G. J. Simitses, 1995, “Delamination Buckling of Flat Laminates”, in *Buckling and Postbuckling of Composite Plates* (G. J. Turvey and I. H. Marshall, editors), Chapman and Hall, 299-328.

36. E. J. Barbero, J. N. Reedy and J. Teply, 1990, "An Accurate Determination of Stresses in Thick Composite Laminates Using a Generalized Plate Theory", *1990 International Journal for Numerical Methods in Engineering* 29,1214.

37. C. M. Dakshinamoorthy and J. N. Reddy, 1998, "Modeling of Laminates Using a Layerwise Element and Enhanced Strains", *1998 International Journal of Numerical Mathematical and Engineering* 43, 755-779.

38. J. Lee, Z. Gurdal and O. H. Griffin Jr., 1992, "A Layer-wise Approach for the Bifurcation Problem in Laminated Composites with Delimitations", *1992 American Institute of Aeronautics and Astronautics Journal* 31(2), 331-338.

39. B. V. Sankar, 1991, "A Finite Element for Modeling Delaminations in Composite Beams", *Computers and Structures* 38, 239-246.

40. M. Krawczuk, W. Ostachowics and A. Zak, 1997, "Dynamic of Cracked Composite Material Structures", *Computational Mechanics* 20, 79-83.

41. S. Hanagud and H. Luo, 1994, "Modal Analysis of a Delaminated Beam", *SEM Spring Conference on Experimental Mechanics*, Baltimore, MD.

42. G. L. Nageshbabu and S. Hanagud, "Delaminations in Smart Composite Structures: a Parametric Study on Vibrations", *1990 Proceedings of the 31st AIAA/ASME/ASCE/AHS/ASCSDM Conference*, Part 4, 2417-2426.

43. M. H. H. Shen and J. E. Grady, 1992, "Free Vibration of Delaminated Beams", *AIAA Journal* 30, 1361-1370.

44. A. K. Pandey, M. Biswas and M. M. Samman, 1991, "Damage Detection Form Changes in Curvature Mode Shapes", *Journal of Sound and Vibration* 145, 321-332.

45. H. F. Lam, J.M. Ko and C. W.Wang, 1995, "Detection of Damage Location Based on Sensitivity Analysis", *Proceedings of the 13th International Modal Analysis Conference*, 1499-1505.

46. J. H. Kim, H. S. Jeon and C. W. Lee, 1992, "Application of the Modal Assurance Criteria for Detecting and Locating Structural Faults", *Proceedings of 10th International Modal Analysis Conference*, 536-540.

47. O. S. Salawu and C. Williams, 1994, "Damage Location Using Vibration Mode Shapes", *Proceedings of the 12th International Modal Analysis Conference*, 933-939.

48. J. Chance, G.R. Tomlinson and K.Worden, 1994, "A Simplified Approach to the Numerical and Experimental Modeling of the Dynamics of a Cracked Beam", *Proceedings of the 12th International Modal Analysis Conference*, 778-785.

49. M. J. Schulz, P. F. Pai and A. S. Abdelnaser, 1996, "Frequency Response Function Assignment Technique for Structural Damage Identification", *Proceedings of the 14th International Modal Analysis Conference*, 105-111.

50. T. W. Lim, 1995, "Structural Damage Detection Using Constrained Eigenstructure Assignment", *Journal of Guidance, Control, and Dynamics* 18, 411-418.

51. M. Sanayei and O. Onipede, 1991, "Damage Assessment of Structures Using Static Test Data", *AIAA Journal* 29, 1174-1179.

52. M. Sanayei, O. Onipede and S. R. Babu, 1992, "Selection of Noisy Measurement Locations for Error Reduction in Static Parameter Identification", *AIAA Journal* 30, 2299-2309.

53. S. W. Doebling, 1996, "Damage Detection and Modal Refinement Using Elemental Stiffness Perturbations with Connectivity", *Proceedings of the AIAA/ASME/AHS Adaptive Structures Forum*, 360-370.

54. D. C. Zimmerman and M. Kaouk, 1994, "Structural Damage Detection Using a Minimum Rank Update Theory", *Journal of Vibration and Acoustics* 116, 222-230.

55. L. D. Peterson, K. F. Alvins, S. W. Doebling and K. C. Park, 1993, "Damage Detection Using Experimentally Measured Mass and Stiffness Matrices", *Proceedings of 34th AIAA/ASME/ASCE/AHS/ASC Structures, Structural Dynamics, and Materials Conference*, 1518-1528.

56. O. S. Salawu and C. Williams, 1993, "Structural Damage Detection Using Experimental Modal Analysis and a Comparison of Some Methods", *Proceedings of the 11th International Modal Analysis Conference*, 254-260.

57. Z. Wang, R.M. Lin and M. K. Lim, 1997, "Structural Damage Detection Using Measured FRF Data", *Computer Methods in Applied Mechanics and Engineering* 147, 187-197.

58. S. K. Thyagarajanm, J. Schulz and P. F. Pai, 1998, "Detecting Structural Damage Using Frequency Response Functions", *Journal of Sound and Vibration* 210, 162-170.

59. H. F. Lan, J.M.Ko and C. W.Wong, 1998, "Localization of Damaged Structural Connections Based on Experimental Modal and Sensitivity Analysis", *Journal of Sound and Vibration* 210, 91-115.

60. H.-Y. Kim, 2003, Vibration-Based Damage Identification Using Reconstructed FRFS in Composite Structures", *Journal of Sound and Vibration* (2003) -59(5), 1131–1146

61. R. P. C. Sampaioa, N. M. M. Maiab and J. M. M. Silva, 1999, "Damage Detection Using the Frequency-Response-Function Curvature Method", *Journal of Sound and Vibration* Volume 226, Issue 5, 7 October 1999, Pages 1029-1042

62. O. S. Salawu, 1997, "Detection of Structural Damage through Changes in Frequency: a Review", *Engineering Structures* 19, 718-723.

63. P. Cawley and R. D. Adams, 1979, "The Location of Defects in Structure from Measurements of Natural Frequencies", *Journal of Strain Analysis* 4, 49-57.

64. D. Sanders, Y. I. Kim and R. N. Stubbs, 1992, "Non-destructive Evaluation of Damage in Composite Structures Using Modal Parameters", *Experimental Mechanics* 32, 240-251.

65. R. Ceravolo and A. D. Stefano, 1995, "Damage Location in Structure through a Connectivistic Use of FEM Modal Analyses", *The International Journal of Analytical and Experimental Modal Analysis 10, 176*.

66. H. T. Banks, D. J. Inman, D. J. Lwo and Y. Wang, 1996, "An Experimentally Validated Damage Detection Theory in Smart Structure", *Journal of Sound and Vibration* 191, 859-880.

67. F. P. Sun, Z. Chaudhry, C. A. Rogers and M. Majmundar, 1995, "Automated Real-time Structure Health Monitoring via Signature Pattern Recognition", *Proceedings of SPIE -The International Society for Optical Engineering Smart Structures and Materials: Smart Sensing, Processing, and Instrumentation* Vol. 1443, 236-243.

68. Z. Chaudhry, T. Joseph, F. Sun and C. Rogers, 1995, "Local-area Health Monitoring of Aircraft via Piezoelectric Actuator/sensor Patches", *Proceedings of SPIE – The International Society for Optical Engineering Smart Structures and Materials Smart Sensing, Processing, and Instrumentation*, Vol. 2443, 268-276

69. Sun, F. P., 1995, "Automated Real-time Structure Health Monitoring via Signature Pattern Recognition", *Proc of the SPIE-Smart Struct and Matls Conf*, 2443,236-247

70. Chaudhry, Z, 1995, "Local-area Health Monitoring of Aircraft via Piezoelectric Acutuator/sensor Patches", *Proc of the SPIE-Smart Struct and Matls Conf*, 2443,268-276

71. Ayres, J W., 1998, "Qualitative Impedance-based Health Monitoring of Civil Infrastructure," *Smart Matls and Struct*, 7(5), 599-605

72. Esteban, J, 1999, "Wave Localization Due to Material Damping", *Computer Methods in Appl Mech and Engrg*, 177(122), 93-107

73. Tseng, K., 2002, "Non-parametric Damage Detection and Characterization Using Smart Piezoceramic Material", *Smart Matls and Struct*, 11(3), 317-329

74. S. C. Gales, W.K. Chiu and J. J. Paul, 1993, "Use of Piezoelectric Films in Detecting and Monitoring Damage in Composites", *Journal of Intelligent Material Systems and Structures* 4, 330-336.

75. S. Egusa and N. Iwasawa, 1996, "Piezoelectric Paints as One Approach to Smart Structural Materials with Health-monitoring Capabilities", *Smart Materials Structures* 7, 438-445.

76. X. H. Jian, H. S. Tzou, C. J. Lissenden, and L. S. Penn, "Damage Detection by Piezoelectric Patches in a Free Vibration Method", *Journal of Composite Materials* 31, 345-359.

77. G. P. Dube, P. C. Dumir and C. Balaji Kumar, 1999, Segmented Sensors and Actuators for Thick Plates and Shells Part I: Analysis Using FSDT, *Journal of Sound and Vibration* (1999) 226(4), 739-753

78. P. C. Dumir, G. P. Dube and C. Balaji Kumar, 1999, "Segmented Sensors and Actuators for Thick Plates and Shells Part II: Parametric Study", *Journal of Sound and Vibration* (1999) 226(4), 755-767

79. S.-E. Park and T.R. Shrout, J. Appl. Phys., 82, (4), 1804 (1997).

80. Wang, C S, 2001, "Structural Health Monitoring from Fiber-reinforded Composites to Steel-reinforced Concrete", *Smart Matls and Struct*, 10(3), 548-552

81. C. H. Keilers, Jr. and F.-K. Chang, 1993, "Damage Detection and Diagnosis of Composites Using Built-in Piezoceramics", *Proceedings of SPIE-The International Society for Optical Engineering Smart Structures and Intelligent System* Vol. 1917, 1009-1015.

82. C. H. Keilers Jr., and F.-K. Chang, 1995, "Identifying Delamination in Composite Beams Using Built-in Piezolectrics: Part I-Experiments and Analysis", *Journal of Intelligent Materials Systems and Structures* 6, 649-663.

83. C. H. Keilers Jr., and F.-K. Chang, 1995, "Identifying Delamination in Composite Beams Using Built-in Piezolectrics: Part II-An Identification Method", *Journal of Intelligent Material Systems and Structures* 6, 664-672.

84. K. Choi, C. H. Keilers, Jr., and F.-.K. Chang, 1994, "Impact Damage Detection in Composite Structures Using Distributed Piezoceramics", *Proceedings of the AIAA/ASME/ASCE/AHS/ASC Structures, Structural Dynamics, and Materials Conference* Vols. 18-20, 118-124.

85. B. S. Shen, M. Tracy, Y.-S. Roh and F.-K. Chang, 1996, "Built-in Piezoelectrics for Processing and Health Monitoring of Composite Structures", *Proceedings of the AIAA/ASME/ASCE/AHS/ASC Structures, Structural Dynamics, and Materials*

Conference, 390-397

86. A. S. Islam and K. C. Cralg, 1994, "Damage Detection in Composite Structures Using Piezoelectric Materials", *Smart Materials and Structures* 3, 318-328.

87. A. C. Okafor, K. Chandrashekhara and Y. P. Jiang, "Delamination Prediction in Composite Structures with Built-in Piezoelectric Devices Using Modal Analysis and Neutral Network", *Smart Materials and Structure* 5, 338-347.

88. P. M. Majumdar and S. Suryanarayan, 1988, "Flexural Vibrations of Beams with Delaminations", *Journal of Sound and Vibration* 125, 441-461.

89. J. Rhim and S. W. Lee, 1995, "A Neural Network Approach for Damage Detection and Identification of Structures", *Computational Mechanics* 16, 437-443.

90. Z. Chaudhry and A. J. Ganino, 1994, "Damage Detection Using Neural Networks: an Initial Experimental Study on Debonded Beams", *Journal of Intelligent Material Systems and Structures* 5, 585-589.

91. H. Luo and S. Hanagud, 1997, "Dynamic Learning Rate Neural Network Training and Composite Structural Damage Detection", *AIAA Journal* 35, 1522-1527.

92. Hou, Z, 2000, "Wavelet-based Approach for Structural Damage Detection." *J of Engrg Mech*, 126(7), 677-683

93. Lin, X. 2001, "Diagnostic Lamb Waves in an Integrated Piezoelectric Sensor/actuator Plate Analytical and Experimental Studies" *Smart Matls and Struct*, 10(5), 907-913

94. Na, W, 2003, "Lamb Waves for Detection Delamination Between Steel Bars and Concrete" *Computer Aided Civil and Infrast Engrg*, 18, 58-63.

95. Lemistre, M, 2001, "Structural Health Monitoring System Based on Diffracted Lamb Wave Analysis by Multiresolution Processing" *Smart Matls and Struct*, 10(3), 504-511

96. Yam, L H, 2003, "Vibration-based Damage Detection for Composite Structures Using Wavelet Transform and Neural Network Identification" *Composite Struct*, 60(4), 403-412

97. Okafor, A C, 1996, "Delamination Prediction in Composite Beams Built-in Piezoelectric Devices Using Modal Analysis and Neural Network" *Smart matls and Struct*, 5(3), 338-347

98. Egusa, S, 1998, "Piezoelectric Paints as One Approach to Smart Structural Materials with Health-monitoring Capabilities" *Smart Matls and Struct*, 7(4), 438-445.

99. Galea, C S, 1993, "Use of Piezoelectric Films in Detecting and Monitoring Damage in Composites" *J of Intell Matl System and Struct*, 4, 683-689

100. A. Ergin, B. Ugurlu, 2004, "Hydroelastic Analysis of Fluid Storage Tanks by Using a Boundary Integral Equation Method", *Journal of Sound and Vibration*, Volume 275, Issues 3-5, 23 August 2004, Pages 489-513

101. S.P. Lim, M. Petyt, 1980, "Free Vibration of a Cylinder Partially Filled with a Liquid", *Proceedings of the International Conference on Recent Advances in Structural Dynamics*, Institute of Sound and Vibration, Southampton University, 7–11 July 1980, pp. 447–455.

102. L.G. Olson and K.J. Bathe, Analysis of fluid–structure interactions, A direct symmetric coupled formulation based on the fluid velocity potential. *Computers and Structures* **21** (1985), pp. 21–32.

103. R. Ohayon and R. Valid, True symmetric variational formulations for fluid–structure interaction in bounded domains-finite element results. In: R.W. Lewis, P. Bettess and E. Hinton, Editors, *Numerical Methods in Coupled Systems*, Wiley, New York (1984), pp. 293–325.

104. H.J.-P. Morand and R. Ohayon. *Fluid Structure Interaction*, John Wiley and Sons, Paris (1995).

105. T. Mazúch, J. Horáček, J. Trnka and J. Veselý, Natural modes and frequencies of a thin clamped–free steel cylindrical storage tank partially filled with water: FEM and measurements. *Journal of Sound and Vibration* **193** (1996), pp. 669–690.

106. Y.L. Zhang, D.G. Gorman and J.M. Reese, 2001, "Finite Element Method for Modeling the Vibration of Initially Tensioned Thin-walled Orthotropic Cylindrical Tubes Conveying Fluid", *Journal of Sound and Vibration* **245** (2001), pp. 93–112.

107. U. Röhr and P. Möller, 2001, "Hydroelastic Vibration Analysis of Wetted Thin-walled Structures by Coupled FE-BE-procedure", *Structural Engineering and Mechanics* **12** (2001), pp. 101–118.

108. G.V. Mysore, S.I. Liapis and R.H. Plaut, 1998, "Dynamic Analysis of Single-anchor Inflatable Dams", *Journal of Sound and Vibration* **215** (1998), pp. 251–272.

109. A. Ergin, W.G. Price, R. Randall and P. Temarel, 1992, "Dynamic Characteristics of a Submerged, Flexible Cylinder Vibrating in Finite Water Depths", *Journal of Ship Research* **36** (1992), pp. 154–167.

110. A. Nestegård, M. Mejlænder-Larsen, 1994, "Hydrodynamic Added Mass of a Floating Vibrating Structure", in: O. Faltinsen, et al. (Eds.), *Hydroelasticity in Marine Technology*, A.A. Balkema, Rotterdam, 1994, pp. 261–272.

111. A. Ergin and P. Temarel, 2002, "Free Vibration of a Partially Liquid-filled and Submerged, Horizontal Cylindrical Shell", *Journal of Sound and Vibration* **254** (2002), pp. 951–965.

112. M. Amabili, M.P. Païdoussis and A.A. Lakis, 1998, "Vibrations of Partially Filled Cylindrical Tanks with Ring-stiffeners and Flexible Bottom", *Journal of Sound and Vibration* **213** (1998), pp. 259–299.

113. F. Kito, 1970, *Principles of Hydro-Elasticity*, Keio University Publications, Tokyo (1970).

114. J.L. Hess and A.M.O. Smith, 1967, "Calculation of Potential Flow about Arbitrary Bodies", In: *D. Küchemann et al. Progress in Aeronautical Sciences* Vol. 8, Pergamon Press, New York (1967), pp. 1–138.

115. J.L. Hess, 1975, "Review of Integral-equation Techniques for Solving Potential-flow Problems with Emphasis on the Surface-source Method", *Computer Methods in Applied Mechanics and Engineering* ***5*** (1975), pp. 145–196.

116. Johannes Wandinger, 2002, "The Virtual Mass Method", Virtual Mass Seminar, MSC Corporation.

117. MSC.Nastran, User's Manual, MSC.Software Corporation, Santa Ana, CA

118. Issac M. Daniel, *Engineering Mechanics of Composite Materials*, Oxford University Press, 1994